

Portland State University

PDXScholar

Mechanical and Materials Engineering Faculty
Publications and Presentations

Mechanical and Materials Engineering

5-6-2022

Characteristics of the Wake of an Inclined Prolate Spheroid in Uniform Shear Flow

Zhe Wang

Hefei University of Technology, Hefei

Jianzhi Yang

Hefei University of Technology, Hefei

Helge I. Andersson

Norwegian University of Science and Technology-NTNU

Xiaowei Wu

Portland State University

Yuxin Wu

Anhui University of Technology

See next page for additional authors

Follow this and additional works at: https://pdxscholar.library.pdx.edu/mengin_fac



Part of the [Mechanical Engineering Commons](#)

Let us know how access to this document benefits you.

Citation Details

Wang, Z., Yang, J., Andersson, H. I., Zhu, X., Wu, Y., Wang, L., & Liu, M. (2022). Characteristics of the wake of an inclined prolate spheroid in uniform shear flow. *Physics of Fluids*, 34(5), 053604.

This Article is brought to you for free and open access. It has been accepted for inclusion in Mechanical and Materials Engineering Faculty Publications and Presentations by an authorized administrator of PDXScholar. Please contact us if we can make this document more accessible: pdxscholar@pdx.edu.



Authors

Zhe Wang, Jianzhi Yang, Helge I. Andersson, Xiaowei Wu, Yuxin Wu, Liping Wang, and Minghou Liu

Characteristics of the wake of an inclined prolate spheroid in uniform shear flow

Cite as: Phys. Fluids **34**, 053604 (2022); <https://doi.org/10.1063/5.0085270>

Submitted: 14 January 2022 • Accepted: 21 April 2022 • Published Online: 06 May 2022

Zhe Wang (王哲),  Jianzhi Yang (杨渐志),  Helge I. Andersson, et al.



View Online



Export Citation



CrossMark

ARTICLES YOU MAY BE INTERESTED IN

[Numerical investigation on the flow around an inclined prolate spheroid](#)

Physics of Fluids **33**, 074106 (2021); <https://doi.org/10.1063/5.0058516>

[Control of the flow around a finite square cylinder with a flexible plate attached at the free end](#)

Physics of Fluids **34**, 027109 (2022); <https://doi.org/10.1063/5.0082181>

[Swimming of an inertial squirmer array in a Newtonian fluid](#)

Physics of Fluids **34**, 053303 (2022); <https://doi.org/10.1063/5.0090898>

APL Machine Learning

Open, quality research for the networking communities

Now Open for Submissions

LEARN MORE



Characteristics of the wake of an inclined prolate spheroid in uniform shear flow

Cite as: Phys. Fluids **34**, 053604 (2022); doi: [10.1063/5.0085270](https://doi.org/10.1063/5.0085270)

Submitted: 14 January 2022 · Accepted: 21 April 2022 ·

Published Online: 6 May 2022



View Online



Export Citation



CrossMark

Zhe Wang (王哲),^{1,2} Jianzhi Yang (杨渐志),^{1,a)} Helge I. Andersson,³ Xiaowei Zhu,⁴ Yuxin Wu (吴玉欣),⁵ Liping Wang (王立平),¹ and Minghou Liu (刘明侯)⁶

AFFILIATIONS

¹Department of Built Environment, Hefei University of Technology, Hefei 230009, China

²Anhui's International Joint Research Center on Hydrogen Safety, Hefei 230009, China

³Department of Energy and Process Engineering, Norwegian University of Science and Technology-NTNU, 7491 Trondheim, Norway

⁴Department of Mechanical and Materials Engineering, Portland State University, Portland, Oregon 97207, USA

⁵School of Energy and Environment, Anhui University of Technology, Maanshan, Anhui 243002, China

⁶Department of Thermal Science and Energy Engineering, University of Science and Technology of China, Hefei, Anhui 230027, China

^{a)} Author to whom correspondence should be addressed: jianzhiy@hfut.edu.cn

ABSTRACT

Flow around an inclined 5:2 prolate spheroid with the incidence angle $\alpha = 45^\circ$ is numerically investigated in a uniform shear flow. The Reynolds number based on the inflow center velocity U_c and the volume-equivalent sphere diameter D_e of the spheroid are considered at $Re = 480, 600, 700$, and 750 . The non-dimensional shear rate K is ranged from 0 to 0.1. Five qualitatively different wake modes are observed, including a new mode characterized by multi-periodic shedding of hairpin vortices with regular rotation of the separation region. In general, the wake transition is suppressed with increasing shear rate. At high shear rates, the flow even reverts from unsteady to steady state at $Re = 480$, which we attributed to the reduction of the local Reynolds number at the leading-edge side of the spheroid. The time-averaged drag/lift coefficients and the Strouhal number increase with increasing the shear rate and the Reynolds number (except for $K = 0$). Finally, the effect of a sign-change of the incidence angle of the prolate spheroid on wake evolution is investigated. A physical exploration of the effect of the sign of the incidence angle and the amount of inlet shear is provided to give deeper insight into the physical mechanisms acting in the wake behind inclined non-axisymmetric bluff bodies in a shear flow.

Published under an exclusive license by AIP Publishing. <https://doi.org/10.1063/5.0085270>

NOMENCLATURE

a	Half-length of the major axis of the spheroid, m	F_s	Side force, N
b	Half-length of the minor axis of the spheroid, m	K	Shear rate, dimensionless
C_d	Drag coefficient, dimensionless	L_x	Length of the computational domain in the x direction, m
C_y or C_l	Lift coefficient, dimensionless	L_y	Length of the computational domain in the y direction, m
C_z or C_s	Side force coefficient, dimensionless	L_z	Length of the computational domain in the z direction, m
$\overline{C_d}$	Time-averaged drag coefficient, dimensionless	P	Pressure, Pa
$\overline{C_l}$	Time-averaged lift coefficient, dimensionless	Q	The Q -function, s^{-2}
$\overline{C_s}$	Time-averaged side force coefficient, dimensionless	Re	Reynolds number, dimensionless
D_e	Volume-equivalent sphere diameter of the spheroid, m	Re_{local}	Local Reynolds number, dimensionless
f	Characteristic frequency, s^{-1}	St	Strouhal number, dimensionless
F_d	Drag force, N	St_p	Primary vortex shedding frequency, dimensionless
F_l	Lift force, N	St_l	Low frequency, dimensionless
		t	Time, s
		t_s	Time step, s

U_c	Inflow center velocity, m s^{-1}
U_x	Velocity in the x direction, m s^{-1}
U_y	Velocity in the y direction, m s^{-1}
U_z	Velocity in the z direction, m s^{-1}
α	Incidence angle, $^\circ$
λ	Aspect ratio, dimensionless
μ	Dynamic viscosity, Pa s
ρ	Density of the fluid, kg m^{-3}
ν	Kinematic viscosity, $\text{m}^2 \text{s}^{-1}$
ω_x	Streamwise vorticity component, s^{-1}
ω_z	Spanwise vorticity component, s^{-1}

I. INTRODUCTION

Wakes generated by a sphere immersed in a non-uniform flow play a significant role in many aero- and hydrodynamic applications. Compared with the sphere wake in a uniform flow,^{1–14} investigations in a non-uniform flow are scarce.^{15–22} Sakamoto and Haniu²⁰ experimentally investigated the formation mechanism and frequency of vortex shedding from a sphere in uniform shear flow at $\text{Re} = 200\text{--}3000$. They found that the critical Reynolds number beyond which vortex shedding from the sphere occurred was lower than that in uniform flow and decreased approximately linearly with increasing the shear rate. Also, the Strouhal number of the hairpin-shaped vortex loops became larger than that in uniform flow and increased with the shear rate. Lee and Wilczak¹⁷ performed a numerical investigation on the effects of shear inlet on wakes behind a sphere using a three-dimensional finite-element method in the range $\text{Re} = 20\text{--}500$. The critical Reynolds number for onset of vortex shedding was found to be lower than that in a uniform flow and varied with the shear rate. Moreover, the vortex shedding frequency also increased with Reynolds number and shear rate. Irregularities of the vortex shedding and oscillations of the vortex detachment location appeared in uniform and low-shear flows at $\text{Re} = 500$ but vanished at higher shear rates. Kim *et al.*¹⁶ numerically investigated the characteristics of laminar flow past a sphere in uniform shear. The effects of inlet shear on the vortical structures, Strouhal number, and time-averaged drag and lift coefficients in the sphere wake were reported. In addition, a hysteresis phenomenon was observed with switching from planar symmetry to asymmetry (or vice versa) depending on the initial condition. However, in many natural and industrial processes, such bluff bodies are non-spherical, and most can be approximated as spheroidal bodies with different aspect ratios such as particles in the fluidized bed²³ and unmanned underwater vehicles.²⁴ Therefore, investigations on the wake behind spheroidal bodies have practical importance. Furthermore, when a spheroidal body is located in the viscous wall boundary layer or a wind-driven ocean current, the resulting flow field is also of practical interest for the motion of tiny particles in a shear flow or inside a narrow pipe. The existence of a bluff body may also affect the flow transition from laminar to turbulent inside a boundary layer.²⁵ Unfortunately, most previous investigations of flow over a prolate spheroid are in uniform flow. This motivates detailed investigations of flow past a spheroid in a shear flow.

Corresponding investigations of the wake behind an inclined prolate spheroid have mostly been performed in the recent decade. A steady flow separation was observed by Zamyshlyayev and Shrager²⁶ in the lee of 10:9 and 5:3 spheroids at $\text{Re}_d = 100$ based on the length of the minor axis of the spheroid when the polar axis was aligned with

the flow, i.e., $\alpha = 0^\circ$. Through direct numerical simulations, El Khoury *et al.*²⁷ numerically studied the wake behind a $\lambda = 6:1$ prolate spheroid when the polar axis was normal to the flow ($\alpha = 90^\circ$) at seven different Reynolds numbers $\text{Re}_d = 50, 75, 100, 150, 200, 250$, and 300 . The aspect ratio λ of the spheroid is taken as $2a/2b$, where “ $2a$ ” denotes the length of the major axis and “ $2b$ ” denotes the length of the minor axis. Except for the two lowest Re_d , hairpin vortices were observed to alternately shed from the two sides of the spheroid. Jiang *et al.*²⁸ investigated the wake behind a 6:1 prolate spheroid at $\alpha = 45^\circ$ incidence angle in detail at $\text{Re}_d = 50, 200$, and 1000 . The wake was still steady and symmetric at two lower Reynolds numbers. For $\text{Re}_d = 1000$, however, only the near-wake was steady and symmetric, whereas the far-wake lost symmetry and exhibited local oscillations. Jiang *et al.*^{29,30} also investigated the transitional wake at $\text{Re} = 3000$, where the wake became unsteady and highly asymmetric from the very beginning, and an in-depth exploration of the main vortical structures was performed. Moreover, Andersson *et al.*³¹ provided an overview of the instabilities, bifurcations, and transitions in the wake over a wide range of Reynolds numbers from 10 to 3000. At a higher $\text{Re}_d = 4000$,³² the resulting wake became highly asymmetric and unsteady. Furthermore, a distinct Kelvin–Helmholtz shear-layer instability was detected. More recently, Wang *et al.*³³ numerically investigated the wake behind a 5:2 prolate spheroid at different Reynolds numbers ($\text{Re} = 300, 500, 700$, and 1000) and incidence angles ($\alpha = 0^\circ\text{--}90^\circ$). In the ranges of Re and α considered, eight flow regimes were identified: (i) steady axisymmetric flow regime (SA), (ii) steady planar symmetric flow regime (SS), (iii) steady asymmetric flow regime (SAS), (iv) periodic planar symmetric flow regime with non-zero mean lift or “Zig-zig-like” mode (Zz-like), (v) periodic asymmetric flow regime with double-sided vortex shedding (PAD), (vi) multi-periodic asymmetric flow regime with double-sided vortex shedding and low-frequency modulation (MPADL), (vii) multi-periodic asymmetric flow regime with single-sided vortex shedding and low-frequency modulation (MPASL), and (viii) weakly chaotic state (WC). A flow regime map in (Re, α) -space was provided.

For a prolate spheroid in a shear flow, corresponding work is rather limited. Hölzer and Sommerfeld³⁴ performed simulations to investigate the effect of the incidence angle ($\alpha = 0^\circ\text{--}180^\circ$) and shear rate ($K = 0, 0.04$, and 0.08) on the drag and lift coefficients of a 3:2 prolate spheroid at some lower Reynolds numbers in a uniform shear, in which $\text{Re} = 0.3, 30, 90$, and 240 . They found that the mean shear induced lift of the spheroid changed direction at approximately $\text{Re} = 90$. Recently, Fillingham *et al.*³⁵ investigated the force coefficients on a prolate spheroid with different aspect ratios ($\lambda = 1, 1.5, 2, 3$, and 5) resting on a smooth surface in a linear shear flow at different incidence angles ($\alpha = 0^\circ\text{--}90^\circ$). New relations were developed for the aerodynamic forces on the prolate spheroidal particle attached to a surface in a linear shear flow. Unfortunately, however, detailed flow field features and vortical structures were not studied in these works.

Some previous works have been performed to investigate the wake behind a prolate spheroid, but almost only considered the case with uniform flow. This idealized situation is believed to give rise to a rather different evolution of the wake than in many actual settings encountered in natural and industrial processes, where a shearing flow is caused by the presence of a solid surface. For the flow past an inclined prolate spheroid in a uniform shear, some questions may arise: What is the effect of inlet shear on the wake evolution of an

inclined prolate spheroid? What is the difference between the wakes in uniform flow and shear flow? What is the effect of inlet shear on the vortex shedding frequency, the drag, and lift coefficients? What is the effect of the direction of incidence of the prolate spheroid on the wake evolution? In order to answer these questions and fill the knowledge gap in the literature, a 5:2 prolate spheroid is considered with the incidence angle $\alpha = +45^\circ$, where the shear rate is varied from $K = 0$ –0.1 and $Re = 480, 600, 700$, and 750 . Unlike in a uniform flow, the sign of the incidence angle is also affecting the wake evolution in a uniform shear flow. Therefore, simulations are also performed for $\alpha = -45^\circ$ at $Re = 480$. This paper is organized as follows: The flow problem and the numerical formulation are described in Sec. II. The wake evolutions and the effects of the uniform shear are presented in Sec. III. Finally, some concluding remarks are provided in Sec. IV.

II. NUMERICAL FORMULATION

A. Governing equations and numerical method

In the present work, the flow around a streamwise inclined prolate spheroid is considered. In a Cartesian coordinate system (x, y, z) , the unsteady incompressible Navier–Stokes (N–S) equations are solved. The N–S equations are as follows:

$$\frac{\partial U_i}{\partial x_i} = 0, \quad (1)$$

$$\frac{\partial U_i}{\partial t} + U_j \frac{\partial U_i}{\partial x_j} = -\frac{1}{\rho} \frac{\partial P}{\partial x_i} + \nu \frac{\partial^2 U_i}{\partial x_j^2}, \quad (2)$$

where $i, j = x, y, z$, ρ is the density of the fluid, ν is the kinematic viscosity, and P is the pressure. U_x , U_y , and U_z are the velocity components in the x -, y -, and z -directions, respectively.

Numerical solutions of the incompressible Navier–Stokes equations are obtained using the finite-volume-based commercial code FLUENT-18.0 (ANSYS, Inc., 2017). This code relies on an unstructured body-fitted grid with collocated pressure and velocity nodes. The numerical algorithm is based on the SIMPLE methodology. A third-order upwind scheme, i.e., QUICK, is used to discretize the convective terms in the momentum equation. A robust second-order implicit backward Euler scheme is used for the transient simulations. The most favorable convergence criteria are set at 10^{-6} for all the flow variables.

B. Computational domain and boundary conditions

As shown in Fig. 1, the case of an inclined prolate spheroid in a linear shear flow is considered. The origin of the coordinate system is located at the geometrical center of the prolate spheroid with the x -, y -, and z -coordinates representing the streamwise, cross-flow, and spanwise directions, respectively. The major axis of the prolate spheroid is at an incidence angle $\alpha = 45^\circ$ with respect to the direction of the inflow U_x , as shown in Fig. 1(a). The aspect ratio λ of the spheroid is

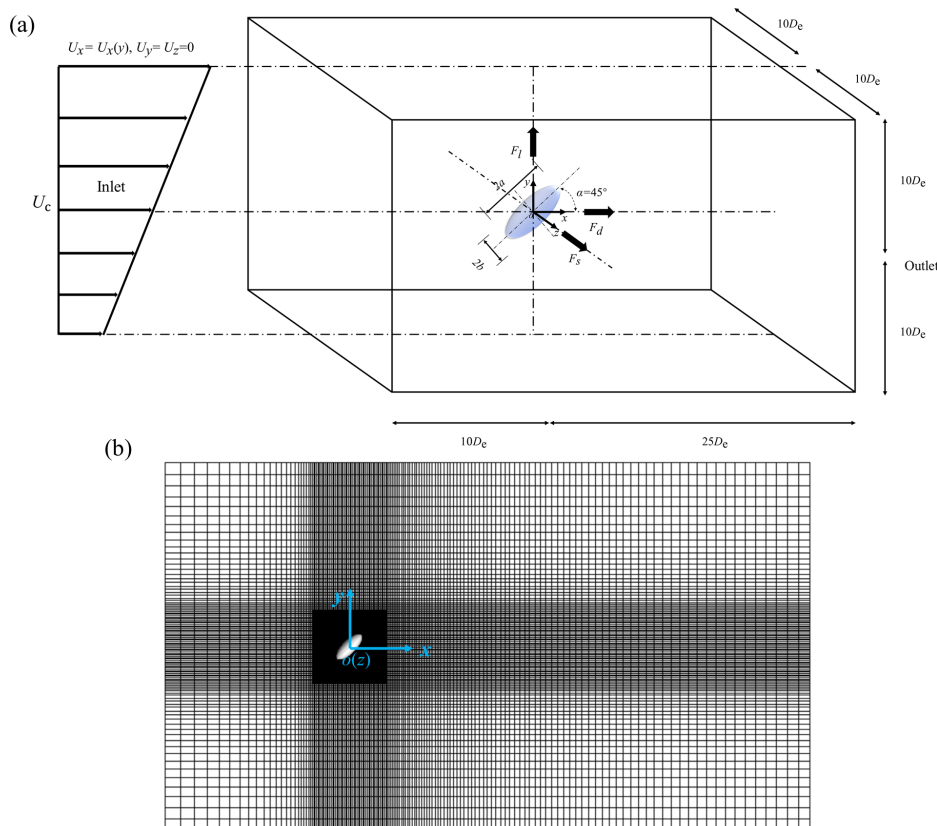


FIG. 1. (a) Sketch of the computational domain and the linearly increasing inflow U_x given in Eq. (6) and (b) the whole mesh at the xy plane.

taken as 5:2. The characteristic length scale of the spheroid is chosen to be the equivalent-sphere diameter

$$D_e = 2(ab^2)^{1/3}, \quad (3)$$

and the characteristic velocity scale is the undisturbed ambient flow velocity at the geometric center of the prolate spheroid, U_c . The Reynolds number based on these characteristic scales is

$$Re = U_c D_e / \nu. \quad (4)$$

We note that in some previous works,^{28,30} the minor length $2b$ of the spheroid is used as the characteristic length for the definition of the Reynolds number, i.e., $Re_d = 2bU_c/\nu$, and $Re = 1.356Re_d$ in the present work.

Aside from that the force coefficients acting on the prolate spheroid are defined as follows:

$$C_d = \frac{F_d}{\frac{1}{2}\rho U_c^2 \frac{\pi}{4} D_e^2}, \quad C_l = \frac{F_l}{\frac{1}{2}\rho U_c^2 \frac{\pi}{4} D_e^2}, \quad C_s = \frac{F_s}{\frac{1}{2}\rho U_c^2 \frac{\pi}{4} D_e^2}. \quad (5)$$

Moreover, F_d , F_l , and F_s indicate the force in the x -, y -, and z -directions, respectively. So $F_d = F_x$, $F_l = F_y$, and $F_s = F_z$ and $C_d = C_x$, $C_l = C_y$, and $C_s = C_z$.

The extents of the computational domain in the x -, y -, and z -directions are $(-10D_e, +25D_e)$, $(-10D_e, +10D_e)$, and $(-10D_e, +10D_e)$, respectively, just as in our previous work.³³ The whole computational domain is partitioned into hexahedral elements. According to the grid-independence study by Wang *et al.*,³³ a grid with about 3.8×10^6 elements turned out to be sufficient to resolve the flow field around a 5:2 spheroid in this Reynolds number range. The mesh in the shear layer and near wake of the spheroid is refined to accurately capture the flow structures. The maximum element thicknesses close to the prolate spheroid surface are approximately $0.01D_e$, the number of elements on the spheroid surface is equal to 4.6834×10^4 , and the total number of elements is about 4.0×10^6 . Figure 1(b) illustrates the whole mesh at the xoy plane.

The inflow at $x = -10D_e$ is prescribed as a unidirectional uniform shear flow

$$\frac{U_x(y)}{U_c} = K \frac{y}{D_e} + 1, \quad U_y = U_z = 0, \quad (6)$$

where the non-dimensional shear rate $K = \partial(U_x/U_c)/\partial(y/D_e)$ is constant all over the inflow boundary since $U_x(y)$ is a linear function of y . Different shear rates K will be considered, ranging from $K=0$ (uniform inflow) to $K=0.1$. A pressure-outlet boundary condition is applied at the downstream boundary at $x = +25D_e$, whereas free-slip boundary conditions are imposed on the four sides of the computational domain. No-slip boundary condition is imposed on the surface of the prolate spheroid.

Finally, a time step independence study for $Re=700$ and $K=0$ has been performed. Three different time steps, i.e., $t_s = 3.2 \times 10^{-5}$, 1.6×10^{-5} , and 1×10^{-6} s, were considered. The mean drag coefficients for $t_s = 3.2 \times 10^{-5}$, 1.6×10^{-5} , and 1×10^{-6} s are 0.576, 0.578, and 0.579, respectively. The time interval for averaging is 8192 time steps. Therefore, the time step of 3.2×10^{-5} s is thought enough for the present problem.

C. Numerical verification

Earlier investigations of the wake behind a spheroid in uniform shear flow are non-existing. Therefore, to demonstrate the reliability of the present numerical approach to simulate bluff bodies in a uniform shear flow, we first considered the flow around a sphere in uniform shear at $Re=300$ for shear rates $K=0, 0.075$, and 0.15 . The number of total mesh elements of the sphere case is 3.12×10^6 , and other numerical setting are the same as the prolate spheroid as introduced in Sec. II B. As mentioned in the work of Kim *et al.*,¹⁶ the symmetric plane becomes fixed plane, i.e., the xoy plane for $K>0$ rather than random plane at $K=0$. The present numerical results have demonstrated this feature, and the wake structures visualized by an iso-surface of Q ³⁶ are shown in Figs. 2(a), 2(c), and 2(e). Furthermore, as shown in Figs. 2(b), 2(d), and 2(f), the non-dimensional frequencies of the vortex shedding, i.e., the Strouhal number $St = fD_e/U_c$, are 0.134, 0.145, and 0.156 at shear rates $K=0$, $K=0.075$, and $K=0.15$, respectively. These St -values for the three cases are nearly the same as the values reported by Kim *et al.*¹⁶ In addition, the maximum differences of time-averaged drag and lift coefficient between present work and Ref. 16 are 1.36% and 6.5%, respectively. A detailed comparison between the numerical results of Kim *et al.*¹⁶ and the present work is summarized in Table I. Therefore, the results of this test case justify the reliability of the present computational approach.

III. RESULTS AND DISCUSSION

In this section, the evolution of the wake of an inclined prolate spheroid ($\alpha = 45^\circ$) is presented for $0 \leq K \leq 0.1$ and $Re=480, 600, 700$, and 750 in Subsections III A–III C. The dependence of the Strouhal number and drag and lift coefficients on the shear rate K and the Reynolds number Re is discussed in Subsection III D. Discussion on the effect of negative vs positive incidence angles on the wake evolution is given in Subsection III E.

A. Wake structure at $Re=480$ and 600

In uniform flow, i.e., $K=0$, the wake of a disk^{37,38} or sphere⁴ at $Re=480$ is in an unsteady planar-symmetric mode with non-zero mean lift, i.e., the “Zig-zig (Zz)” mode. The wake structure behind the spheroid is illustrated by iso-surfaces of Q and streamwise vorticity ω_x , as shown in Figs. 3(a) and 3(b). Due to the incidence angle, the hairpin vortices are shedding in a fixed vertical direction rather than in an arbitrary direction as in the wake of a sphere, as shown by Wang *et al.*³³ The similar phenomenon was also reported for an inclined disk.^{39,40} Moreover, in the near wake, the vortex loops are inclined due to the effect of the incidence angle and eventually become perpendicular to the streamwise direction as the wake develops in the downstream, as shown in Figs. 3(a) and 3(b). The diagrams of $C_d - C_y$ and $C_z - C_y$, shown in Figs. 3(c) and 3(d) appear as a single loop and a vertical line, respectively, thereby proving the strict periodicity of the vortex shedding and the symmetry of the wake structure. The time histories of drag and lift coefficients in Fig. 4(a) show regular sinusoidal variations, which are consistent with the single dominant peak in the frequency spectra in Fig. 4(b), which correspond to the primary vortex shedding frequency $St=0.199$.

The Zig-zig (Zz) mode is found to persist even in the presence of a moderately shear inflow, as shown in Fig. 5 for $K=0.05$. The wake structure visualized in Figs. 5(a) and 5(b) is still symmetric about the xoy plane, but the vortex loops are inclined in the far wake, which can

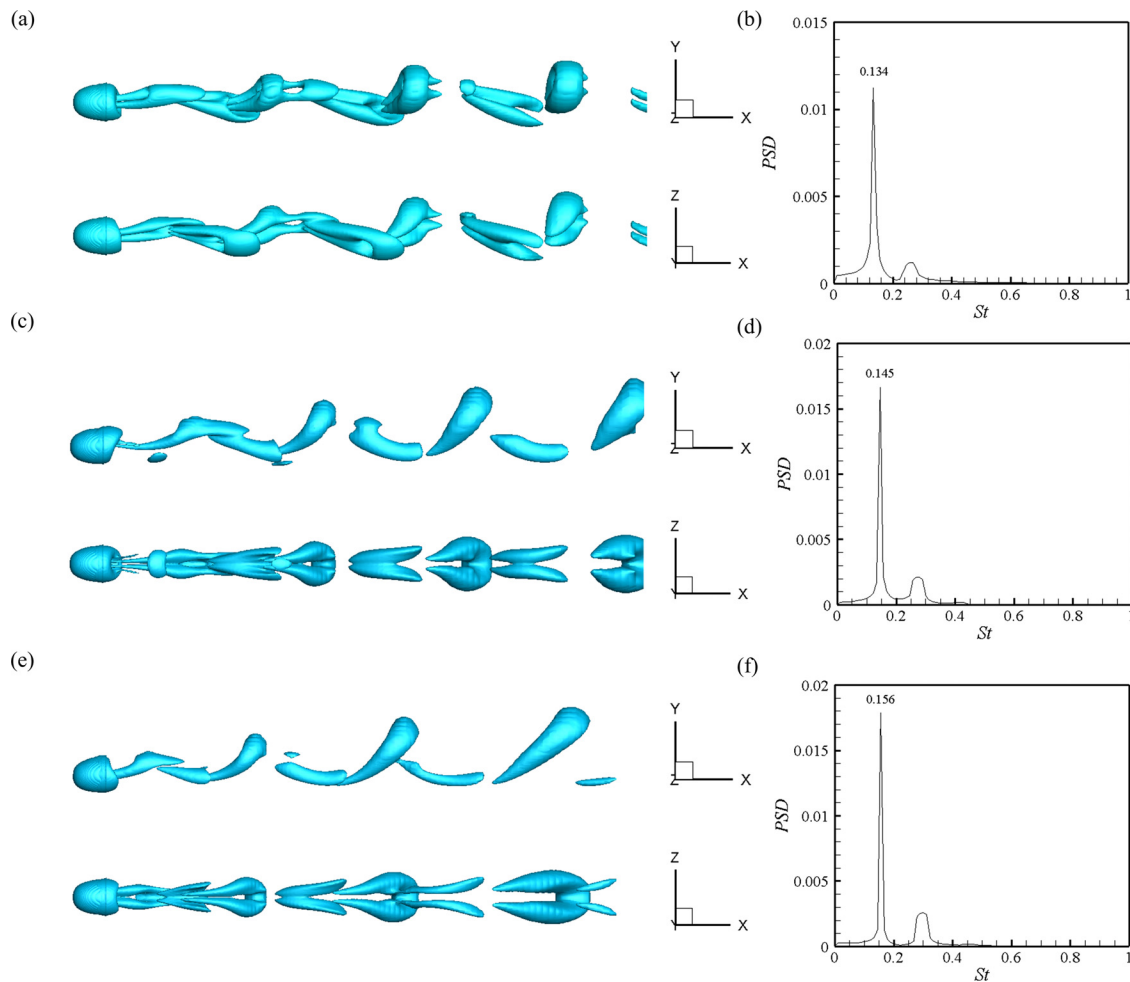


FIG. 2. Flow past a sphere at $Re = 300$. (a), (c), and (e) Wake structure characterized by the iso-surface of Q ($QD_e^2/U_0^2 = 2.5 \times 10^{-3}$) and (b), (d), and (f) frequency spectrum of the drag coefficient. (a) and (b) $K = 0$, (c) and (d) $K = 0.075$, and $K = 0.15$.

TABLE I. The comparison of the numerical results between Ref. 16 and the present work for a sphere at $Re = 300$ and $K = 0, 0.075$, and 0.15 .

		Kim <i>et al.</i> ¹⁶	Present work	Relative error %
$K = 0$	St	0.134	0.134	0.00
	$\overline{C_d}$	0.661	0.670	1.36
	$\overline{C_l}$	0.068	0.072	5.88
$K = 0.075$	St	0.145	0.145	0.00
	$\overline{C_d}$	0.667	0.676	1.35
	$\overline{C_l}$	0.068	0.072	5.88
$K = 0.15$	St	0.156	0.157	0.64
	$\overline{C_d}$	0.674	0.680	0.89
	$\overline{C_l}$	0.070	0.074	5.71

be attributed to the effect of inflow shear. The time histories of drag and lift coefficients in Fig. 4(c) still show sinusoidal oscillations. However, according to the frequency spectra in Fig. 4(d), the primary vortex shedding frequency $St = 0.236$ is substantially higher than in the case of a uniform inflow shown in Fig. 4(b). The higher shedding frequency in the presence of mean shear somehow resembles the increasing St observed with increasing Re in the case with uniform inflow. It can, therefore, be speculated if the Strouhal number and the drag and lift coefficients are determined by a local Reynolds number ($Re_{local} = \frac{\rho U_{\mu} D_s}{\mu}$) rather than by the nominal Re . This point of view will be further discussed in Sec. III E.

It is particularly interesting to observe that the wake flow changes from an unsteady back to a steady state with planar symmetry when K is further increased to 0.075 , as shown in Fig. 6. This phenomenon can be attributed to the obvious decrease in the local Reynolds number at

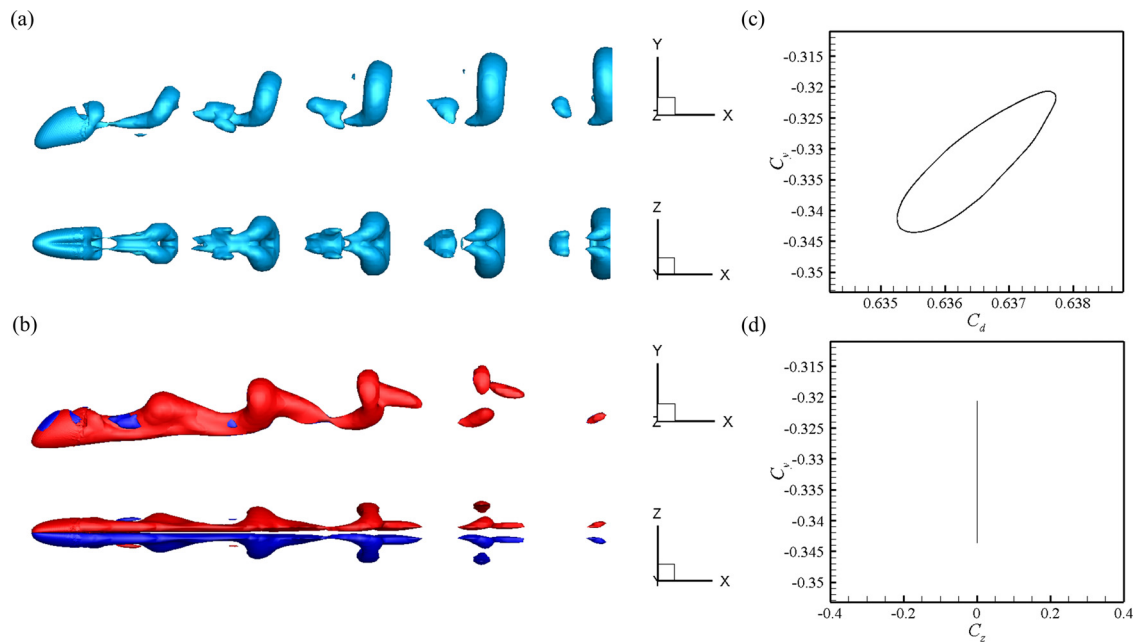


FIG. 3. Unsteady planar-symmetric flow regime (Zz) at $Re = 480$ and $K = 0$: (a) iso-surfaces of Q (two orthogonal views), $QD_e^2/U_c^2 = 2.2 \times 10^{-3}$, (b) iso-surfaces of stream-wise vorticity (two orthogonal views), $\omega_x D_e/U_c = \pm 0.14$, (c) $C_d - C_y$ diagram, and (d) $C_z - C_y$ diagram.

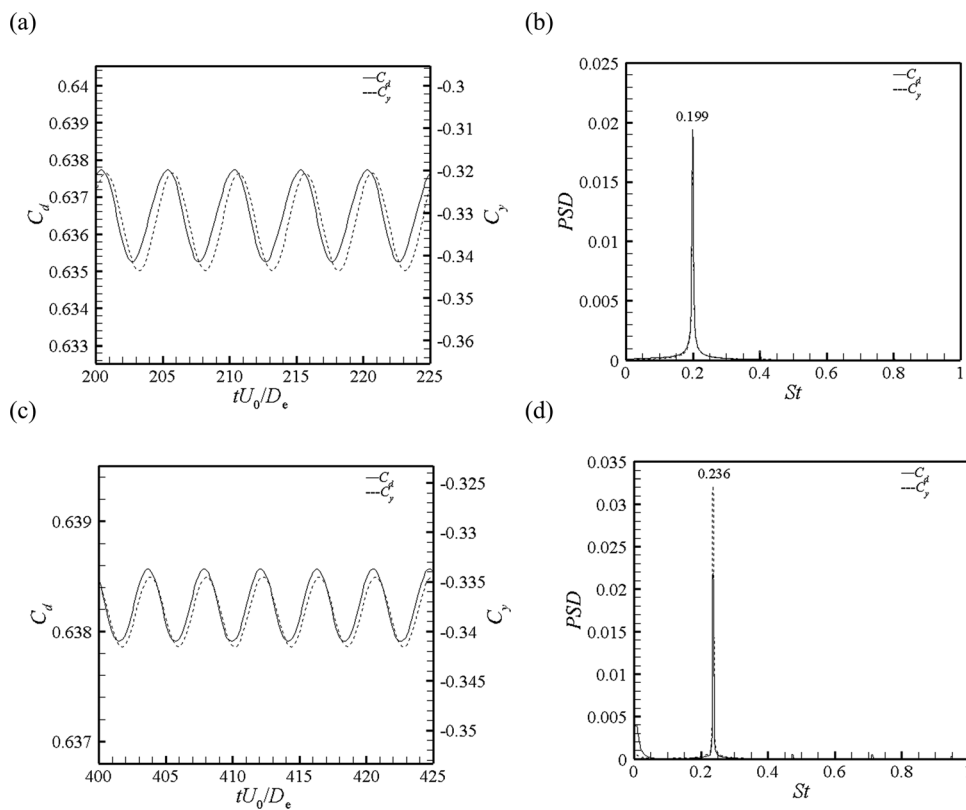


FIG. 4. (a) and (c) Time histories of the drag and lift coefficients and (b) and (d) corresponding frequency spectra of C_d and C_y at $Re = 480$. (a) and (b) Uniform inflow $K = 0$ and (c) and (d) shear inflow $K = 0.05$. The solid and dashed lines represent C_d and C_y , respectively.

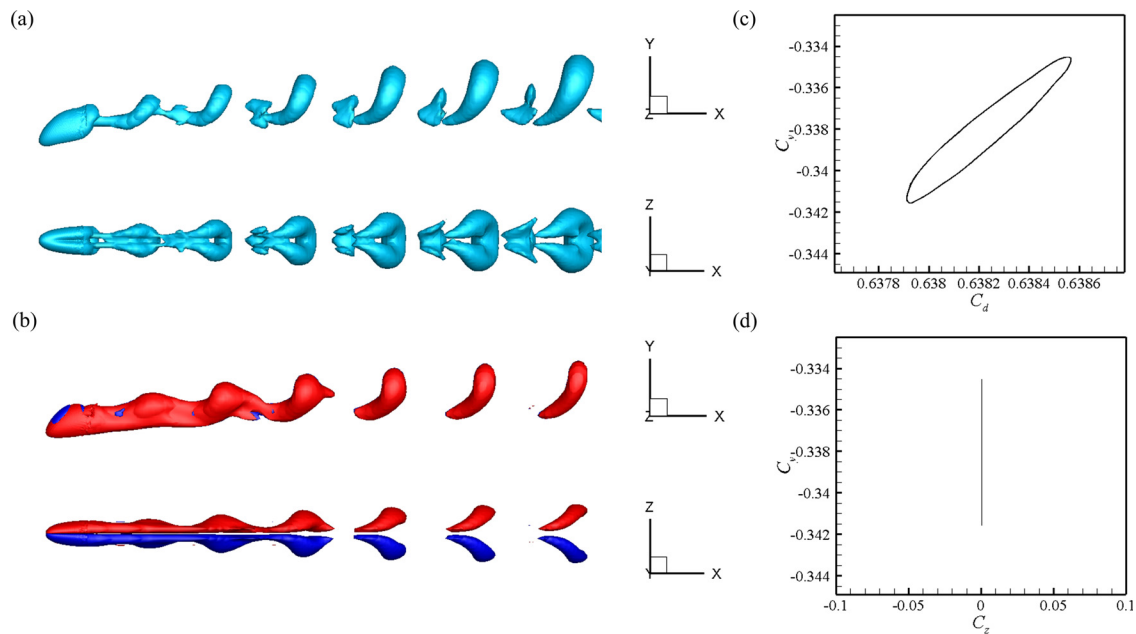


FIG. 5. Unsteady planar-symmetric flow regime (Zz) at $Re = 480$ and $K = 0.05$: (a) iso-surfaces of Q (two orthogonal views), $QD_e^2/U_c^2 = 2.2 \times 10^{-3}$, (b) iso-surfaces of streamwise vorticity (two orthogonal views), $\omega_x D_e/U_c = \pm 0.14$, (c) $C_d - C_y$ diagram, and (d) $C_z - C_y$ diagram.

the leading-edge side of the prolate spheroid. The observed reversal from an unsteady to a steady wake is different from the behavior of the wake of a sphere^{16,20} or a disk.³⁷

At the somewhat higher $Re = 600$, the wake structures for different inlet shear rates K are all unsteady with planar symmetry about the geometrical mid-plane $z = 0$. The wake structures at $K = 0$, 0.05 , and 0.1 are, respectively, presented in Figs. 7(a), 7(c), and 7(e), and it is obvious to note that in the far downstream, the vortex loops with respect to the y -direction are also inclined and the incidence angle of

the vortex loops is increased with increasing K , indicating the inclination of the vortex loop is associated with the presence of inflow shear. Moreover, with the increase in K , the vortex shedding frequency is also increased, and thus, more vortex loops are observed at the same downstream distance. Despite the modified shape of the corresponding $C_d - C_y$ diagrams in Figs. 7(b), 7(d), and 7(f), the close-loop shape is maintained as a result of the periodicity of the vortex shedding.

The time histories of drag and lift coefficients at $Re = 600$, together with the corresponding frequency spectra are provided in Fig. 8. With the increase in K , the oscillation of the drag coefficient is smoother indicating the flow tends to become comparatively steady, as shown in Figs. 8(a), 8(c), and 8(e). The Strouhal number is increasing as the shear rate K increases, similarly as the results for $Re = 480$ shown in Fig. 4. These results show that the characteristics of the wake behind the inclined 5:2 spheroid are controlled by two dimensionless parameters: the Reynolds number (Re) and the shear rate (K). Aside from that a secondary harmonic frequency is also observed, and the peak value is gradually decreased with increasing shear rate.

B. Wake structure at $Re = 700$

The structure and evolution of the wake at different inlet shear rates K at $Re = 700$ become qualitatively different from those observed at the somewhat lower Reynolds numbers; see Subsection III A. As shown in Figs. 9(a) and 9(b), the wake structure loses its symmetry at $K = 0$. Moreover, small oscillations of the vortex loop in the spanwise direction can also be observed, although the size of the vortex loops remains the same. The symmetry breaking occurs mainly at the leg of the hairpin vortex, and the hairpin head remains relatively steady and symmetric. With uniform inflow, i.e., $K = 0$, the trajectories in the $C_d - C_y$ diagram in Fig. 9(c) are filling a leaf-shaped area, which

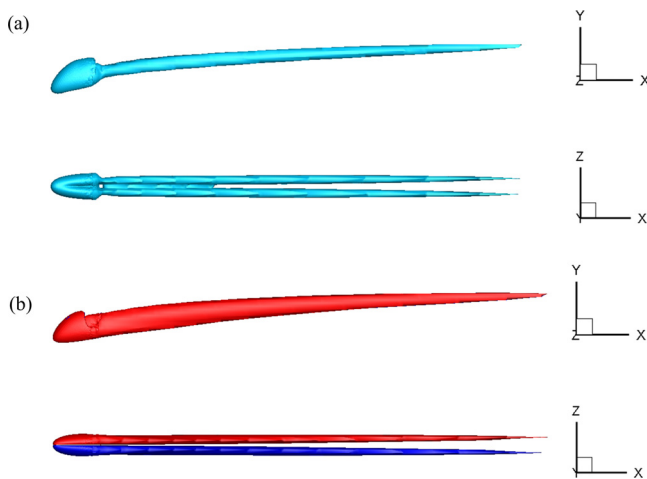


FIG. 6. Steady planar-symmetric flow regime (SS) at $Re = 480$ and $K = 0.075$: (a) iso-surfaces of Q (two orthogonal views), $QD_e^2/U_c^2 = 2.2 \times 10^{-3}$ and (b) iso-surfaces of streamwise vorticity (two orthogonal views), $\omega_x D_e/U_c = \pm 0.14$.

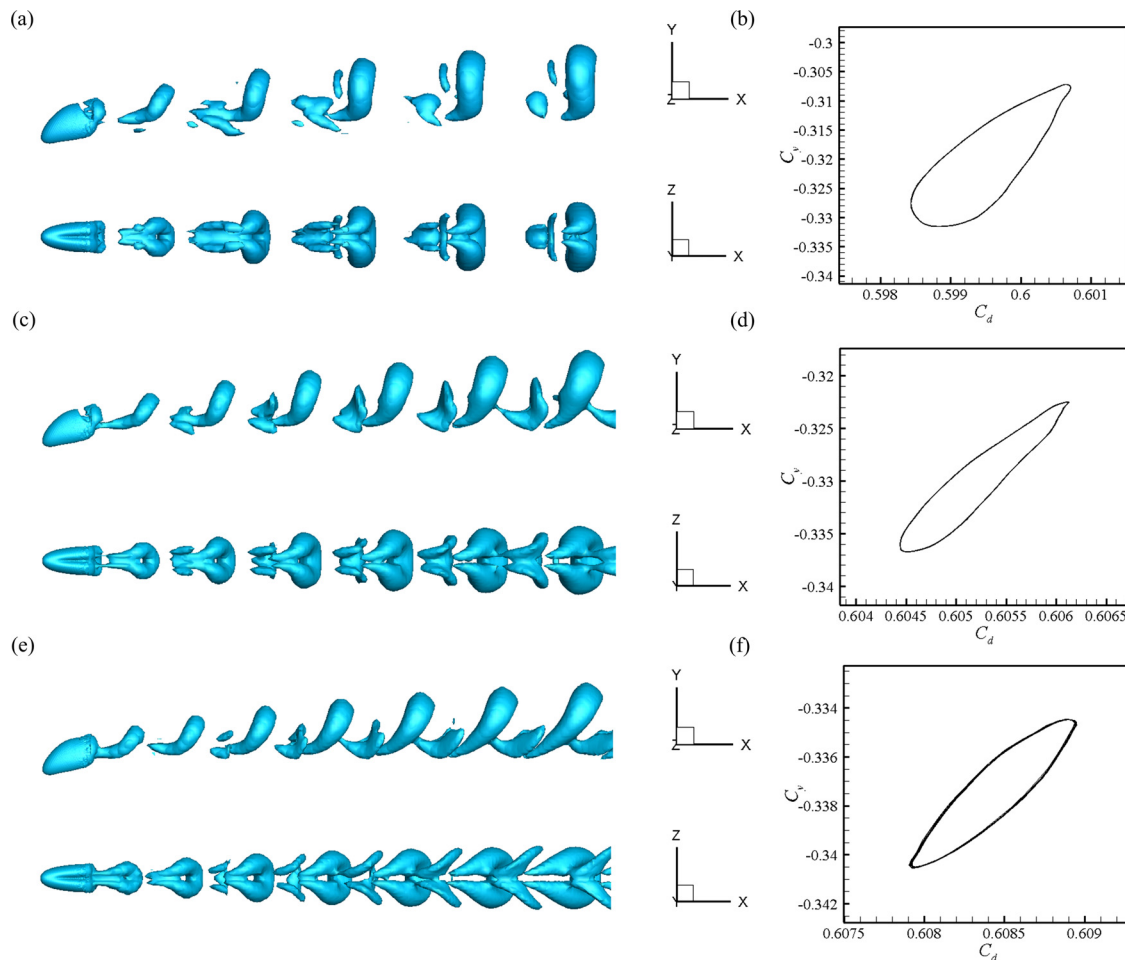


FIG. 7. Unsteady planar-symmetric flow regime (Zz) at $Re = 600$ and $K = 0$ (upper), 0.05 (middle), and 0.1 (lower): (a), (c), and (e) iso-surfaces of Q (two orthogonal views), $QD_0^2/U_c^2 = 1.4 \times 10^{-3}$, and (b), (d), and (f) $C_d - C_y$ diagram.

resembles the shape of the unique trajectory in Fig. 7(b), thereby reflecting that a certain regularity is still retained and indicating a quasi-periodicity of the vortex shedding.³⁸ The $C_z - C_y$ diagram in Fig. 9(d) is no longer a straight vertical line at $C_z = 0$, indicating a broken symmetry of the wake structure, which gives rise to an alternating spanwise force component with zero mean. Thus, this wake mode is referred to as the quasi-periodic asymmetric state (QPA). In the presence of a low shear inflow at $K = 0.025$, the phase diagram and the wake structure (not shown here for brevity) are very similar to those in the uniform flow.

Time histories of drag and lift coefficients and the corresponding frequency spectra at $Re = 700$ and $K = 0$ are shown in Fig. 10. As shown in Fig. 10(a), the lift coefficient still exhibits a sinusoidal-like variation with an almost constant amplitude. The oscillations of the drag coefficient, however, show a periodical variation of amplitude, which is modulated at a low frequency. As shown in Fig. 10(b), in addition to the primary vortex shedding frequency, $St_p = 0.200$, a low frequency, $St_l = 0.036$, is also observed. This lower frequency is about 1/6th of the primary vortex shedding frequency, in agreement with the

time history of the drag coefficient, i.e., every a low-frequency cycle includes six primary cycles. The presence of the low frequency might be related to a secondary instability associated with temporal evolution of the wake structure.⁴¹ For a column or a row of square cylinders, the similar secondary frequency is also observed.^{42–44}

With shear rate further increasing, the wake flow regime changes from the unsteady asymmetric state to an unsteady planar symmetric mode at $K = 0.05$ and 0.075 (not shown for brevity), as shown in Figs. 11(a) and 11(b). A similar phenomenon was also reported for uniform shear flow past a sphere,¹⁶ which is attributed to the fixed vortex detachment point on the high-velocity side that keeps the balance between the supply and emission of vorticity within the vortex formation region.²⁰ Therefore, the regular vortex shedding persists up to a higher Reynolds number in a uniform shear flow. The force coefficients' phase diagrams are plotted in Figs. 11(c) and 11(d), in which a closed single loop and the straight path clearly indicate the flow periodicity and symmetry. The time histories of the drag and lift coefficients are shown in Fig. 12(a). The oscillations of the lift coefficient are sinusoidal with a single amplitude, while the drag coefficient also

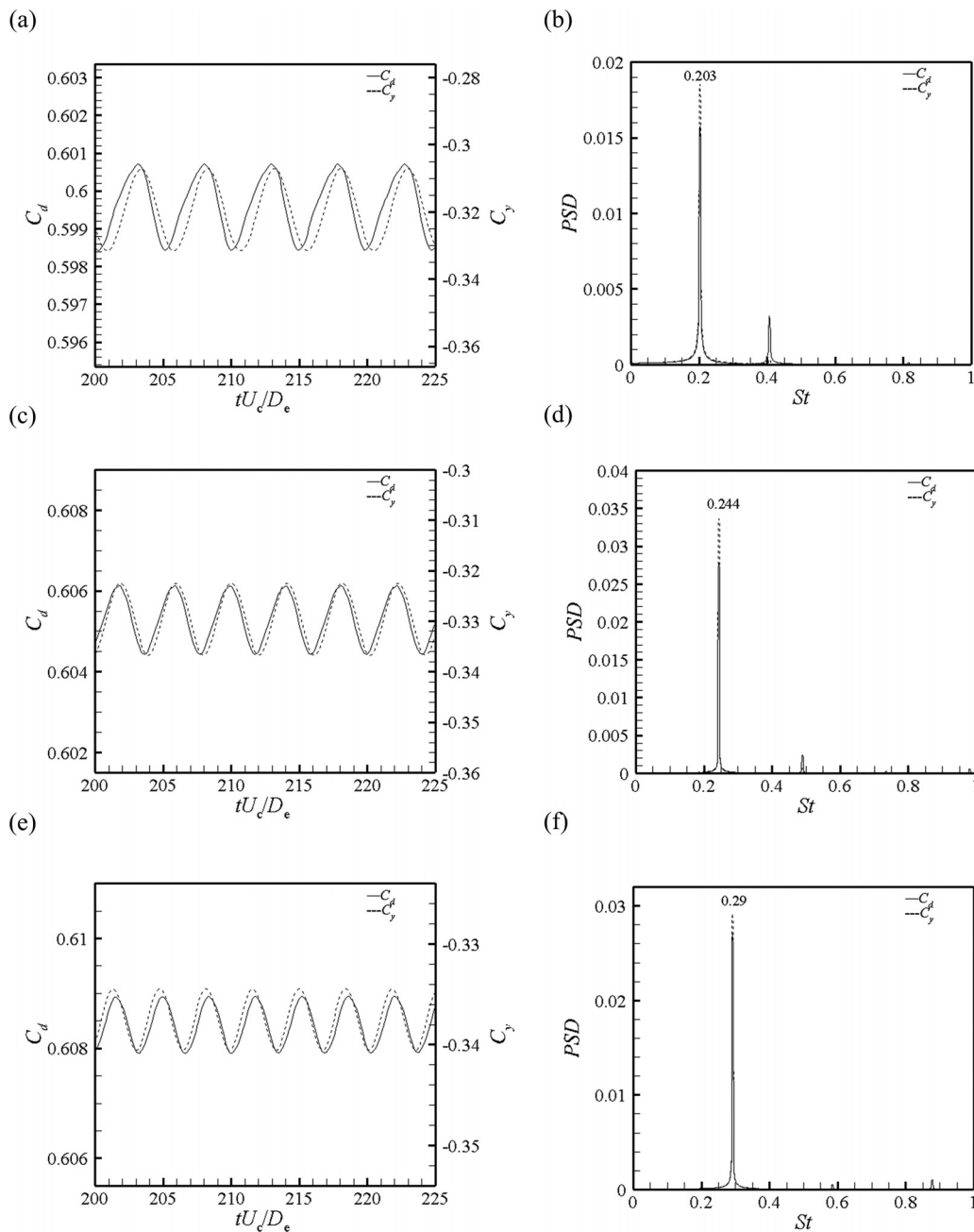


FIG. 8. (a), (c), and (e) Time histories of the drag and lift coefficients, and (b), (d), and (f) the corresponding frequency spectra of C_d and C_y at $Re = 600$. (a) and (b) $K = 0$, (c) and (d) $K = 0.05$, and (e) and (f) $K = 0.1$. The solid and dashed lines represent C_d and C_y , respectively.

varies periodically but with a flattened wavy peak. The modest oscillations on the broadened peak are also related to the higher frequencies at $St \approx 0.50$ and ≈ 0.75 as shown in Fig. 12(b).

When the shear rate is further increased to $K = 0.1$, the wake structure again loses planar symmetry, as shown in Figs. 13(a) and 13(b). This might be due to an increase in the local Reynolds number at the high-velocity side, similarly as in the case of a sphere.¹⁶ The location of

the shedding of vortex loops varies in time along the azimuthal direction, but the size of the hairpin vortex is fundamentally independent of time. It is important to recall that this type of wake structure has never reported in the case of uniform flow. The quite complex shape of the $C_d - C_y$ diagram in Fig. 13(c) reflects the multi-periodic flow. Therefore, the new wake mode is called “multi-periodic shedding of the hairpin vortex mode with regular rotation of the separation

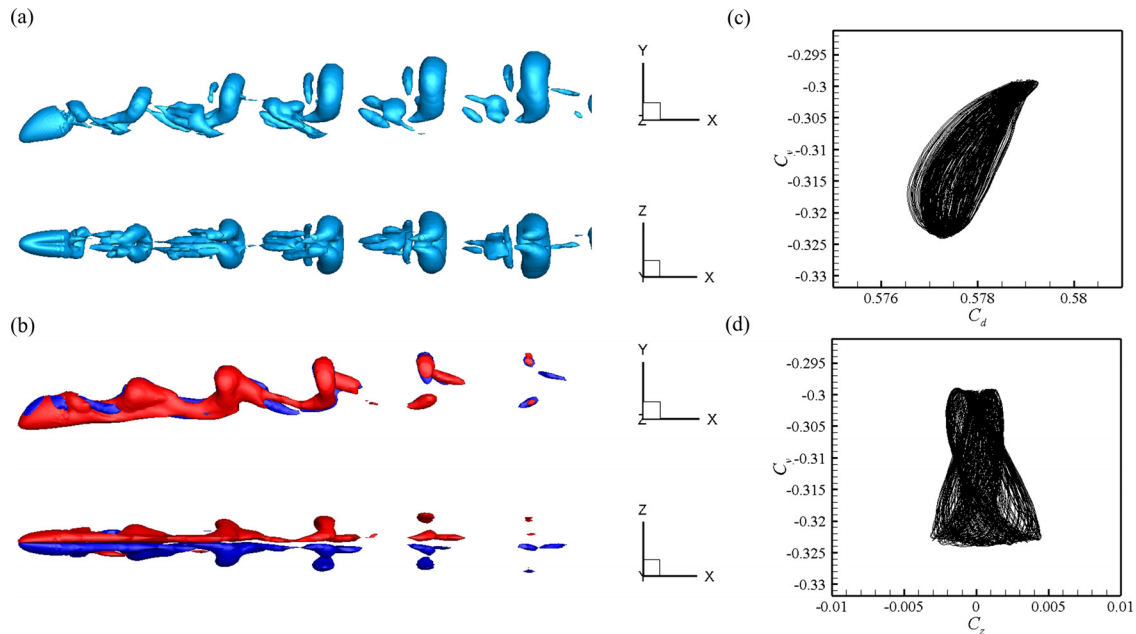


FIG. 9. Quasi-periodic asymmetric flow regime (QPA) at $Re = 700$ and $K = 0$, (a) iso-surfaces of Q (two orthogonal views), $QD_e^2/U_c^2 = 1.03 \times 10^{-3}$, (b) iso-surfaces of streamwise vorticity (two orthogonal views), $\omega_x D_e / U_c = \pm 0.14$, (c) $C_d - C_y$ diagram, and (d) $C_z - C_y$ diagram.

region (MPRRS mode).⁷ Moreover, the shape of the $C_z - C_y$ diagram in Fig. 13(d) reflects the oscillations of the vortex loop in the spanwise z -direction.

The time histories of drag and lift coefficients and the corresponding frequency spectra are shown in Figs. 14(a) and 14(b). The oscillations of the drag and lift coefficients are modulated by a low frequency, $St_l = 0.061$, which is close to 1/5th of the primary frequency, $St_p = 0.302$. Spanwise oscillations of the vortex loops can be observed in Fig. 15(a), which shows the time history of the side-force coefficient. The periodic oscillations of C_z around $C_z = 0$ are modulated at the lower frequency, $St_{z,l} \approx 0.03$. This phenomenon can be explained by

the rotation of the location of the detachment of vortex shedding. Moreover, the lower frequency is also captured by the frequency spectra of drag and lift coefficients shown in Fig. 14(b). To further illustrate the spanwise variation of the wake at the new wake mode, a time sequence of the wake evolutions over a low-frequency period is depicted in Fig. 15(b), which corresponds to the time history marked by the dashed square frame in blue shown in Fig. 15(a). It is noted that the whole wake oscillates about the $z = 0$ plane, which is consistent with the oscillations of the side force coefficient C_z . The location of the shedding of the hairpin vortex varies periodically in time, which is consistent with the low-frequency period of the side force coefficient,

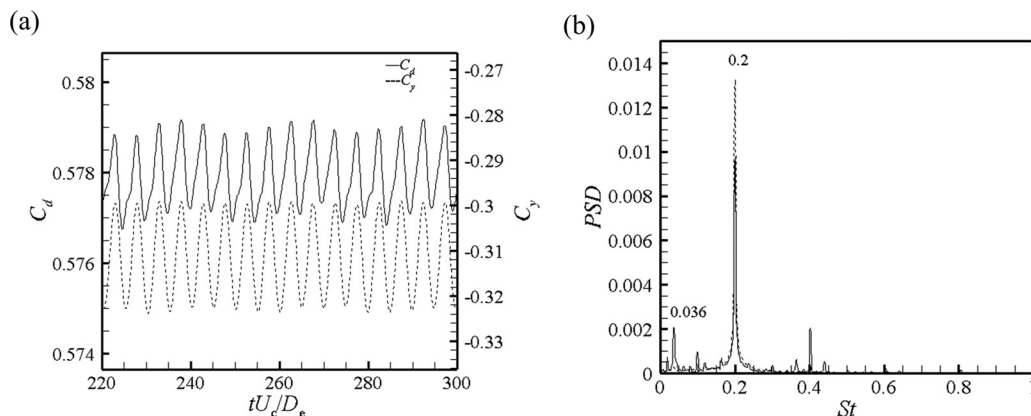


FIG. 10. (a) Time histories of the drag and lift coefficients and (b) the corresponding frequency spectra of C_d and C_y at $Re = 700$ and $K = 0$. The solid and dashed lines represent C_d and C_y , respectively.

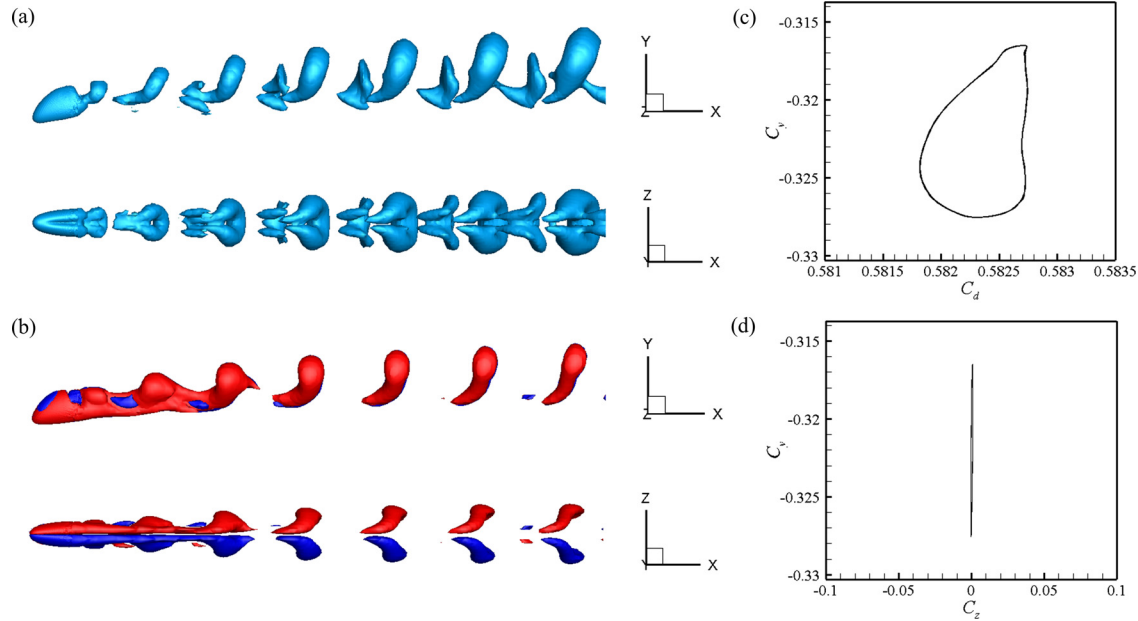


FIG. 11. Unsteady planar symmetric flow regime (Zz) at $Re = 700$: $K = 0.05$, (a) iso-surfaces of Q (two orthogonal views), $QD_e^2/U_c^2 = 1.03 \times 10^{-3}$, (b) iso-surfaces of streamwise vorticity (two orthogonal views), $\omega_x D_e/U_c = \pm 0.14$, (c) $C_d - C_y$ diagram, and (d) $C_z - C_y$ diagram.

i.e., $St_{z,l} = 0.029$. Three different vortex loops are labeled “M,” “L,” and “R,” where M indicates that the vortex loop is symmetric about $z = 0$, L indicates that the vortex loop tilts to the left, and R indicates that the vortex loop tilts to the right. It is noteworthy that the tilt direction of vortex loops in between two consecutive vortex loops marked by M is the same.

C. Wake structure at $Re = 750$

At $Re = 750$, the wake structures for all shear rates considered are asymmetric due to the higher Reynolds number. The wake structures and the $C_d - C_y$ diagrams at $K = 0$ and 0.05 shown in Fig. 16 are

similar to those at $Re = 700$. Although the wake structure in Figs. 16(a) and 16(c) is asymmetric, a certain recovery of the symmetry of the hairpin vortices is observed at $K = 0.05$ as compared with the uniform inflow case. The time histories of the drag and lift coefficients and the corresponding frequency spectra at $K = 0$ and 0.05 are shown in Fig. 17. It is obvious that the oscillations of the drag coefficient are more irregular and also modulated a low frequency at this higher Reynolds number, as shown in Figs. 17(a) and 17(c). At $K = 0$, each low-frequency cycle is nearly comprised of six primary cycles, which is consistent with frequency spectra, in which a low frequency, $St_l = 0.034$, is nearly 1/6th of the primary vortex shedding frequency, $St_p = 0.189$, as shown in Fig. 17(b). The irregular of oscillations of drag

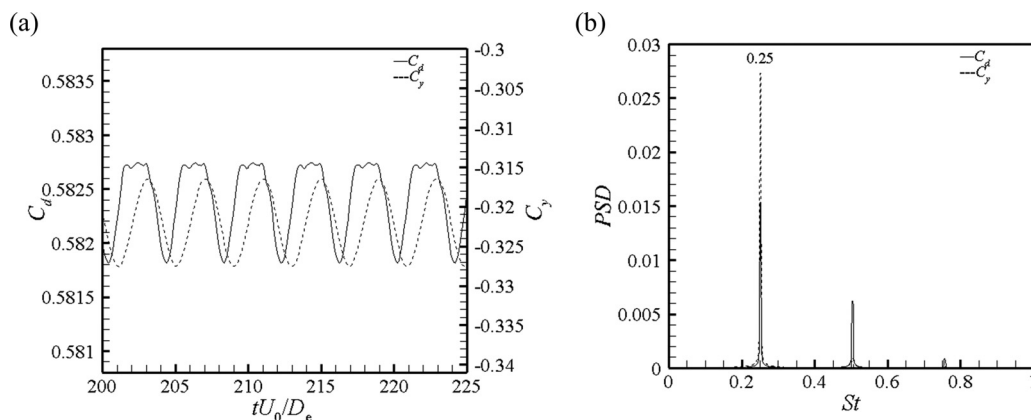


FIG. 12. (a) Time histories of the drag and lift coefficients and (b) the corresponding frequency spectra of C_d and C_y at $Re = 700$ and $K = 0.05$. The solid and dashed lines represent C_d and C_y , respectively.

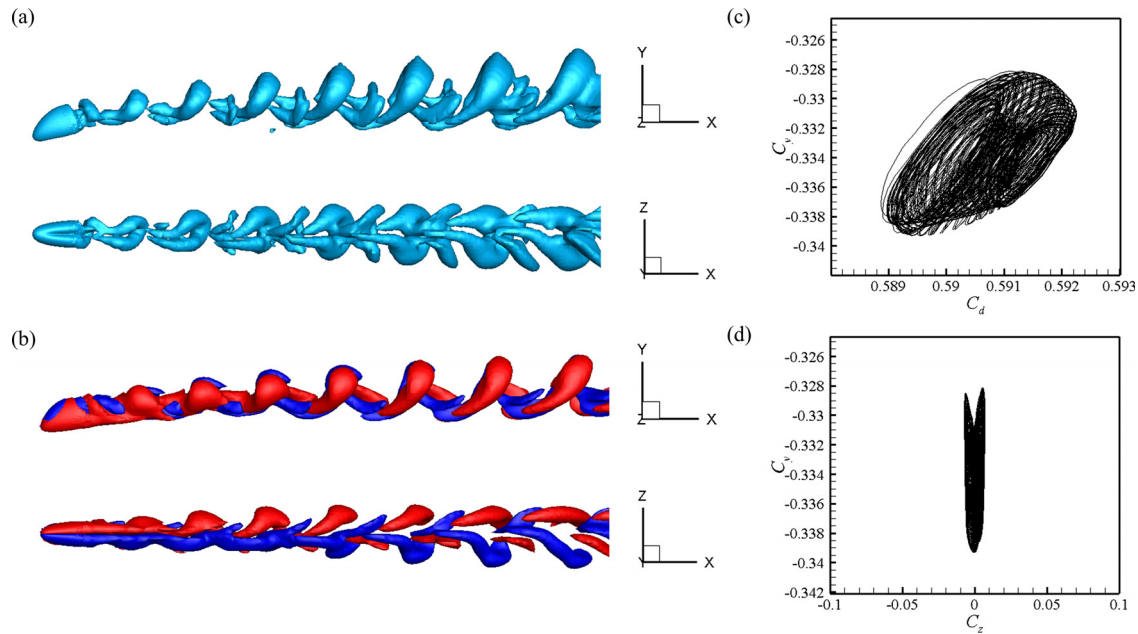


FIG. 13. Multi-periodic shedding of the hairpin vortex mode with regular rotation of the separation region ("MPRRS") at $Re = 700$ and $K = 0.1$: (a) iso-surfaces of Q (two orthogonal views), $QD_e^2/U_c^2 = 1.03 \times 10^{-3}$, (b) iso-surfaces of streamwise vorticity (two orthogonal views), $\omega_x D_e/U_c = \pm 0.14$, (c) $C_d - C_y$ diagram, and (d) $C_z - C_y$ diagram.

and lift coefficients indicates multi-periodicity and a weakly chaotic state. For $K = 0.05$, the oscillations of the drag and lift coefficients with the low-frequency modulation, in which a low-frequency period includes three primary vortex shedding periods, in Fig. 17(c) are more regular, and both are increased compared to the results at $K = 0$. All vortex shedding frequencies are increased, as shown in Fig. 17(d). A primary vortex shedding, $St_p = 0.253$, is observed, and a low-frequency is also captured, which is close to 1/3rd of the primary frequency. With further increase in the shear rate K , the new wake MPRRS mode is also captured at $K = 0.075$ and 0.1 . This observation

indicates that the wake structure becomes more irregular, and the symmetry is again broken. The wake structure and diagrams of drag and lift coefficients at $K = 0.075$ are shown in Fig. 18. Compared to the $C_d - C_y$ diagram at $K = 0.05$, the diagram at $K = 0.075$ in Fig. 18(b) is much more irregular.

To summarize, the wake regimes for flow over an inclined prolate spheroid ($\alpha = 45^\circ$) at $Re = 480, 600, 700$, and 750 in uniform shear flow with shear rate $K = 0-0.1$ comprise five qualitatively different wake modes: the steady-state (SS) mode, Zig-zig (Zz) mode, quasi-periodic asymmetric mode (QPA), multi-periodic asymmetric mode

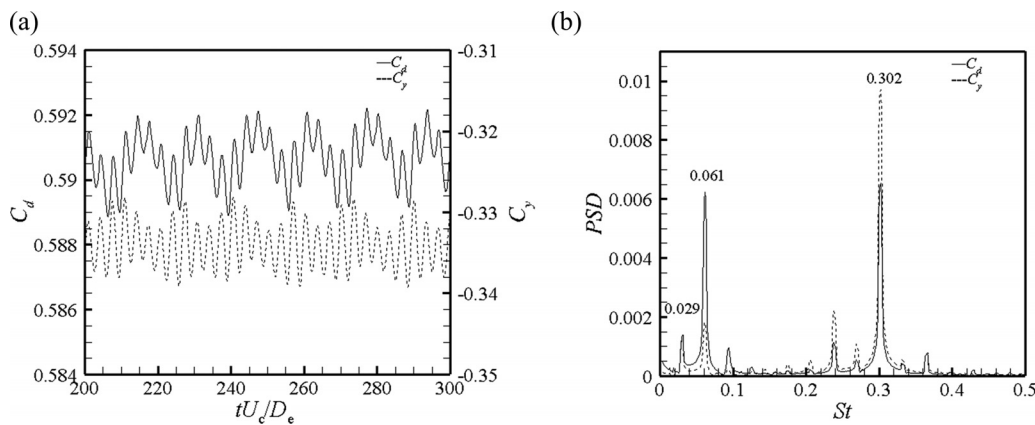


FIG. 14. (a) Time histories of the drag and lift coefficients and (b) the corresponding frequency spectra of C_d and C_y at $Re = 700$ and $K = 0.1$. The solid and dashed lines represent C_d and C_y , respectively.

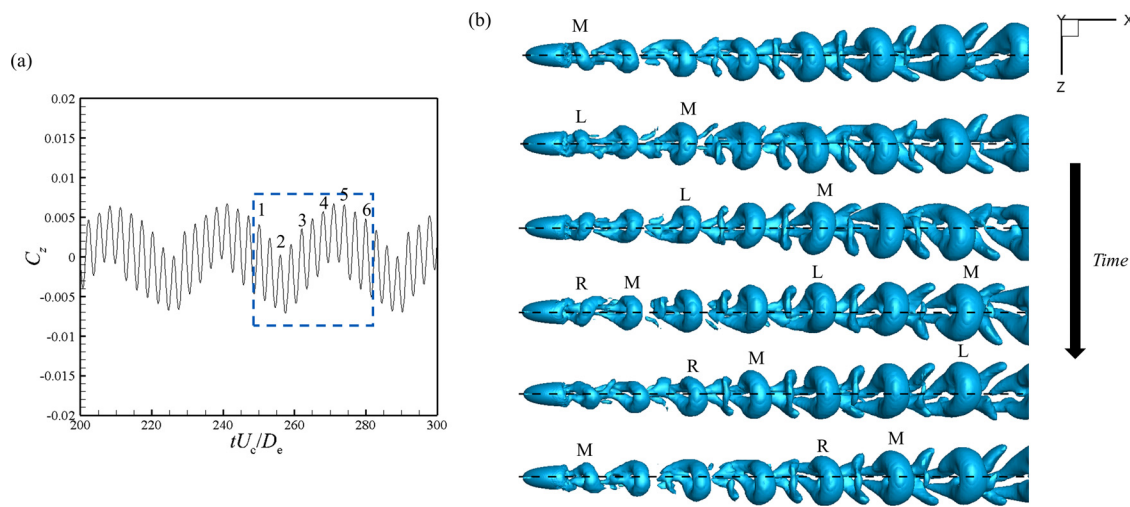


FIG. 15. (a) Time history of the side force coefficient C_z , in which the dashed square frame in blue marks a low-frequency period, and the numbers “1–6” indicate the instants at which the flow fields in (b) are obtained and (b) time sequence of the wake evolution characterized by an iso-surface of Q ($QD_e^2/U_c^2 = 1.03 \times 10^{-3}$) at $Re = 700$ and $K = 0.1$, at the instants indicated at (a). The time interval between two consecutive pictures is $6.8D_e/U_c$. Three different hairpin vortex loops are labeled M, L, and R, respectively. The black dashed line indicates the position of the symmetry plane at $z = 0$.

(MPA), and multi-periodic shedding of the hairpin vortex mode with a regular rotation of the separation region (MPRRS) mode. The occurrence of these wake modes depends on the Reynolds number and the shear rate, as summarized in Table II. For an inclined prolate spheroid, the effect of the increase in the inflow shear rate on the wake transition

is quite complex due to the slender shape of the prolate spheroid. At the lower Reynolds numbers, the increase in inlet shear suppresses shedding of hairpin vortices even though the flow changes from unsteady to steady at $Re = 480$ and $K = 0.075$ and 0.1 . This can be attributed to the abrupt decrease in the local Reynolds number at the

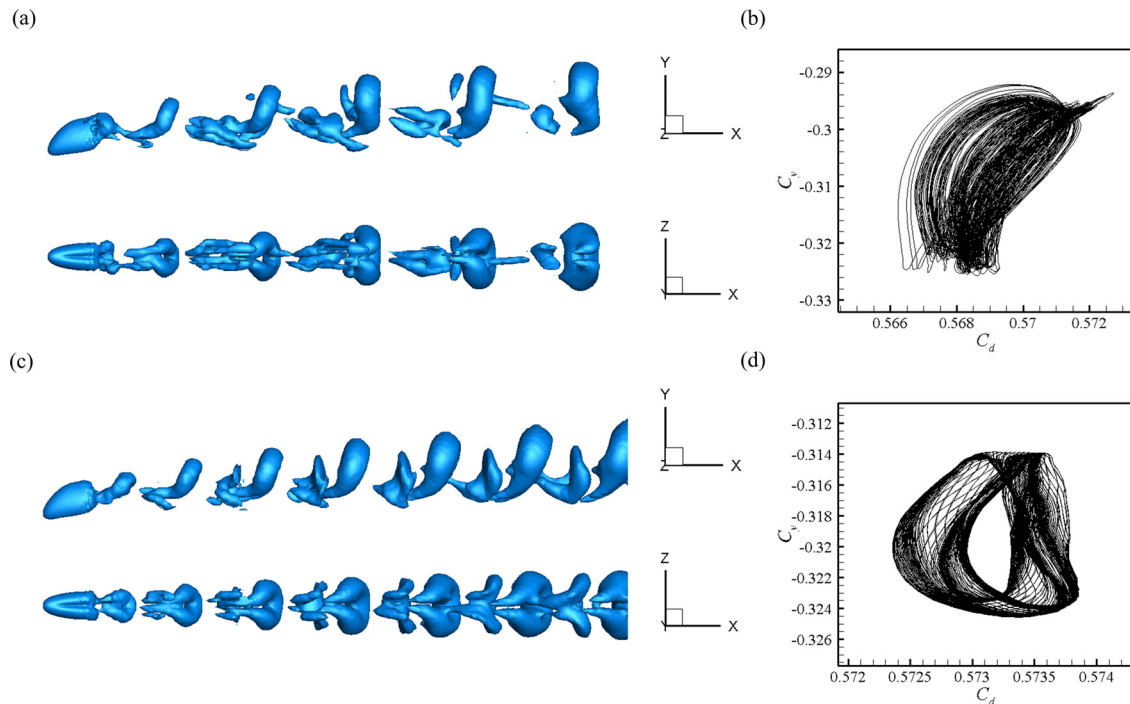


FIG. 16. Multi-periodic asymmetric flow regime (MPA) at $Re = 750$ with different inflow: (a) and (b) $K = 0$ and (c) and (d) $K = 0.05$. (a) and (c) Iso-surfaces of streamwise vorticity (two orthogonal views), $QD_e^2/U_c^2 = 9 \times 10^{-4}$, and (b) and (d) $C_d - C_y$ diagram.

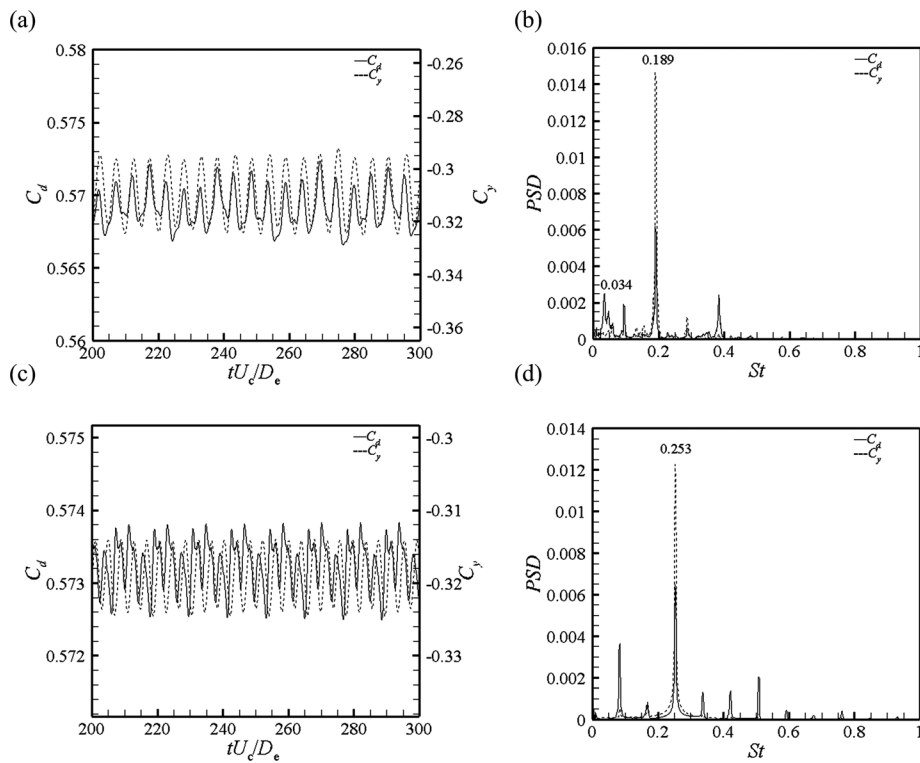


FIG. 17. (a) and (c) Time histories of the drag and lift coefficients, and (b) and (d) the corresponding frequency spectra of C_d and C_y at $Re = 750$. (a) and (b) $K = 0$, and (c) and (d) $K = 0.05$. The solid and dashed lines represent C_d and C_y , respectively.

leading-edge side of the prolate spheroid. When the Reynolds number becomes sufficiently high and the shear rate is small, such as at $Re = 700$, increasing the shear rate also suppresses the shedding of hairpin vortices. The wake flow changes from the unsteady

asymmetric state to an unsteady planar-symmetric state. This phenomenon can be attributed to the steady supply and emission of vorticity, which make the regular vortex shedding cease up to a higher Reynolds number in a uniform shear flow than in uniform flow.

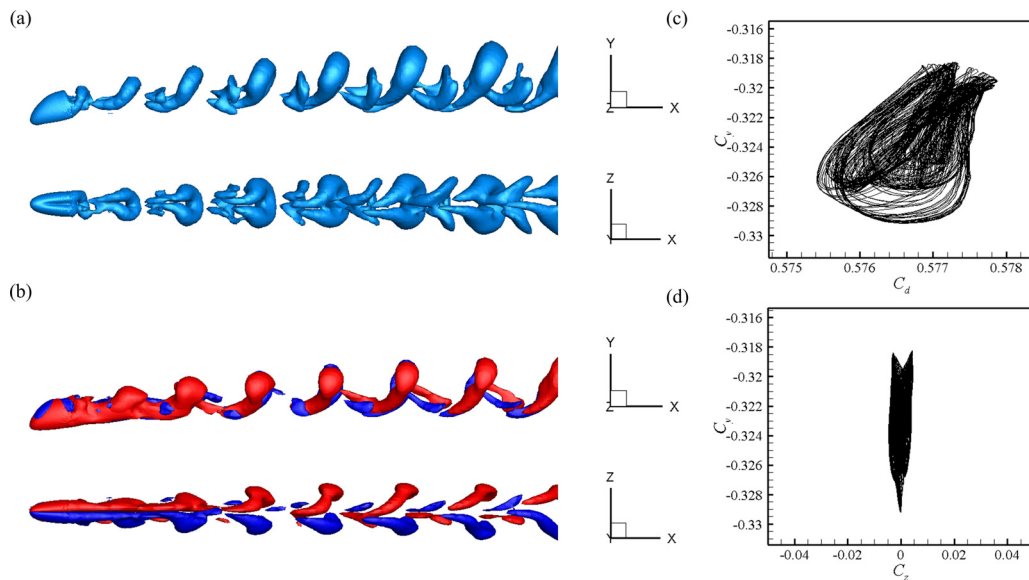


FIG. 18. Multi-periodic shedding of the hairpin vortices mode with regular rotation of the separation region (MPRRS) at $Re = 750$ and $K = 0.075$: (a) iso-surfaces of Q (two orthogonal views), $QD_e^2/U_0^2 = 9 \times 10^{-4}$, (b) iso-surfaces of streamwise vorticity (two orthogonal views), $\omega_x D_e/U_0 = \pm 0.135$, (c) $C_d - C_y$ diagram, and (d) $C_z - C_y$ diagram.

TABLE II. Wake flow regimes depending on the Reynolds number Re and inlet shear rate K .

Re	K				
	0	0.025	0.05	0.075	0.1
480	Zz	Zz	Zz	SS	SS
600	Zz	Zz	Zz	Zz	Zz
700	QPA	QPA	Zz	Zz	MPRRS
750	MPA	MPA	MPA	MPRRS	MPRRS

With further increase in the shear rate, the flow returns to an unsteady asymmetric state, which can be attributed to an increase in the local Reynolds number at the high-velocity side.

D. Drag and lift coefficients and vortex shedding frequency

Time-averaged drag and lift coefficients at different Reynolds numbers and inlet shear rates are shown in Fig. 19. With increasing Reynolds number, the absolute value of both drag and lift coefficients decreases, which is consistent with observations in previous works.^{33,45,46} In contrast, with increasing shear rate, the absolute value of both drag and lift coefficients increases, similarly as if the Reynolds number in uniform flow is reduced. Moreover, due to the wake structure keeping unsteady planar asymmetry for all shear rates at $Re = 600$, the time-averaged drag and lift coefficients almost linearly change with K . However, for $Re = 480, 700$, and 750 , the wake structure or flow state is changed at $K = 0.075$ – 0.1 , which leads to both time-averaged drag and lift coefficients that are no longer linearly change at high shear rates. The corresponding effect of the Reynolds number and inlet shear on the Strouhal number St , i.e., the non-dimensional vortex shedding frequency, is displayed in Fig. 20(a).

Except for the uniform inflow case $K = 0$, the Strouhal number increases with increasing Reynolds number, similarly as in the sphere wake.¹⁶ The Strouhal number is increasing almost linearly with increasing shear rate, similarly as the Reynolds number increases in a uniform flow. For $K = 0$, i.e., uniform inflow, the Strouhal number first increases and thereafter decreases with further increasing Reynolds number. It can be attributed to the gradually more chaotic state at a higher Re .

To further examine the effect of the Reynolds number and shear rate on the variation of the Strouhal number, the Strouhal number is normalized by the Strouhal number at $K = 0$ for different Reynolds numbers, as shown in Fig. 20(b). It should be noted that $St_K/St_{K=0}$ increases almost linearly with K at all four Reynolds numbers considered. Therefore, a simple correlation in terms of the Reynolds number and shear rate is then proposed as follows:

$$St/St_{K=0} = 1 + A \cdot K, \quad (7)$$

where $A = \left(\frac{Re}{646.58}\right)^{5.79} + 3.57$. First, we performed the linear fit by the data points for various Re and acquired different values of the slope “ A ” for all Re by the drawing software of Origin. Then we performed the non-linear fit to build the relation between A and Re . Finally, Eq. (6) could be obtained. As shown in Fig. 20(b), the simple correlation fits very well with the numerical data points with maximum deviation 3.54% observed at $Re = 750$ and $K = 0.025$.

E. The effect of negative vs positive incidence angle on the wake evolution

For flow past an inclined prolate spheroid in uniform flow,³¹ a sign change of the incidence angle α only mirrors the wake topology and inverts the direction of lift force. With a shear inflow, however, a sign change of α will obviously lead to a qualitatively different wake evolution. We have hitherto considered the wake flow behind the 5:2 prolate spheroid with a positive incidence angle of $\alpha = +45^\circ$ relative

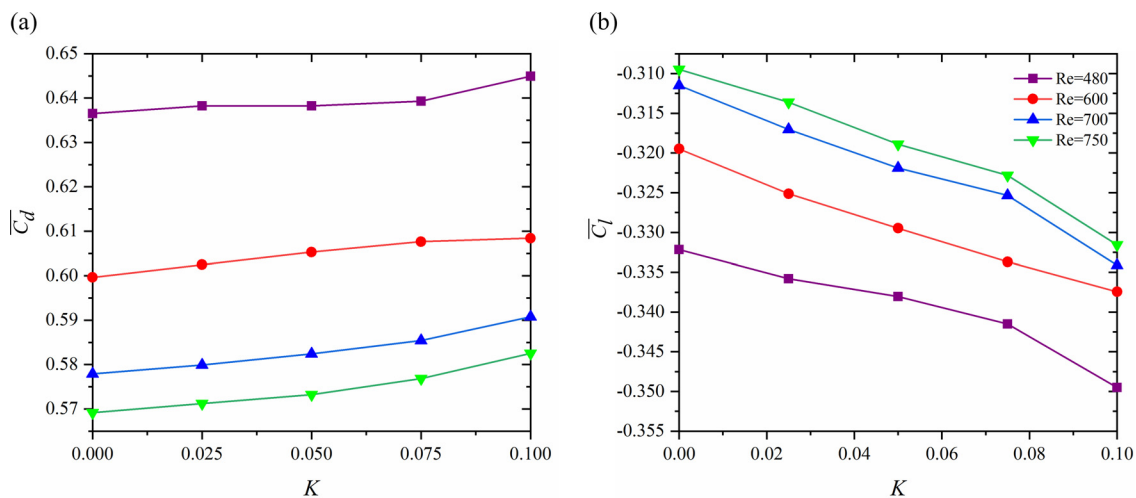


FIG. 19. Variations of the time-averaged drag and lift coefficients at different Reynolds numbers and shear rates. (a) $\overline{C_d}$, (b) $\overline{C_l}$. $Re = 480$, —■—; $Re = 600$, —●—; $Re = 700$, —▲—; $Re = 750$, —▼—.

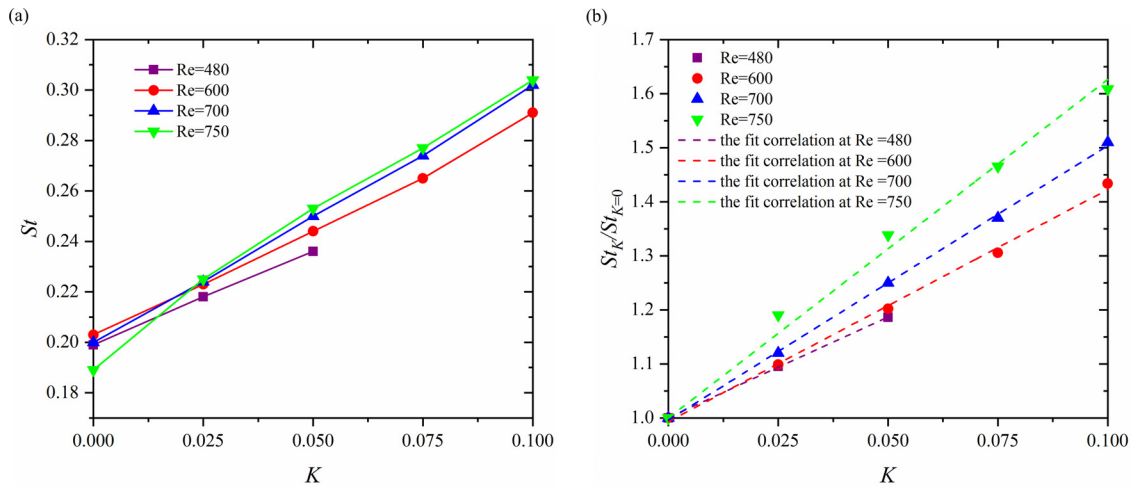


FIG. 20. Variations of the Strouhal number at different Reynolds numbers and shear rates. (a) St and (b) $St_K/St_{K=0}$. The symbols denote the numerical results, and the dashed lines are the fit correlation in Eq. (6). Violet squares and violet dashed lines at $Re = 480$; —●— and —■—, — at $Re = 600$; —●— and —▲—, — at $Re = 700$; —▼— and —, — at $Re = 750$.

to the inflow; see Fig. 1. In this subsection, the wake evolution behind the same prolate spheroid, but with negative incidence angle $\alpha = -45^\circ$, will be explored. For the sake of brevity, this study is confined to the single Reynolds number of $Re = 480$.

Let us recall from Sec. III A that the wake transition at this Reynolds number and $\alpha = +45^\circ$ is suppressed at high shear rates and the flow reverted from an unsteady back to a steady state for $K = 0.075$ and 0.1 , i.e., the critical Reynolds number for onset of vortex shedding increases with increasing shear rate. However, with negative incidence angle $\alpha = -45^\circ$, vortex shedding behind the present spheroid is observed for all shear rates considered in Fig. 21. Moreover, with increasing shear rate, the wake mode is developed from periodic to a quasi-periodic state, i.e., the wake transition is advanced, as shown in Fig. 22. These observations suggest that the critical Reynolds number for occurrence of vortex shedding is reduced with increasing K . A similar tendency has also been observed for flow past a sphere^{17,20} and

ascribed to the steady supply and emission of vorticity within the vortex formation region in uniform shear flow.²⁰ In the present case, however, the vortex shedding always occurs at the low-speed side of the spheroid, contrary to in the sphere wake. Compared to the wake at $\alpha = +45^\circ$, the inclination of the hairpin vortices in Fig. 21 is still affected by both the sign of the incidence angle and the inlet shear K . Moreover, vortex shedding always occurs at the trailing-edge side of the prolate spheroid, and the direction of vortex shedding is determined by the sign of the incidence angle. These findings are supported by simulations at $Re = 400$ and $K = 0.1$ with $\alpha = \pm 45^\circ$, which showed that the wake is still steady for $\alpha = +45^\circ$ as shown in Fig. 23(a), whereas the wake flow developed into an unsteady state for $\alpha = -45^\circ$ as shown in Fig. 23(b).

Drag and lift coefficients and the Strouhal number for two different deflection directions $\alpha = \pm 45^\circ$ are shown in Fig. 24. In the case of negative incidence angle $\alpha = -45^\circ$, the drag coefficient decreases

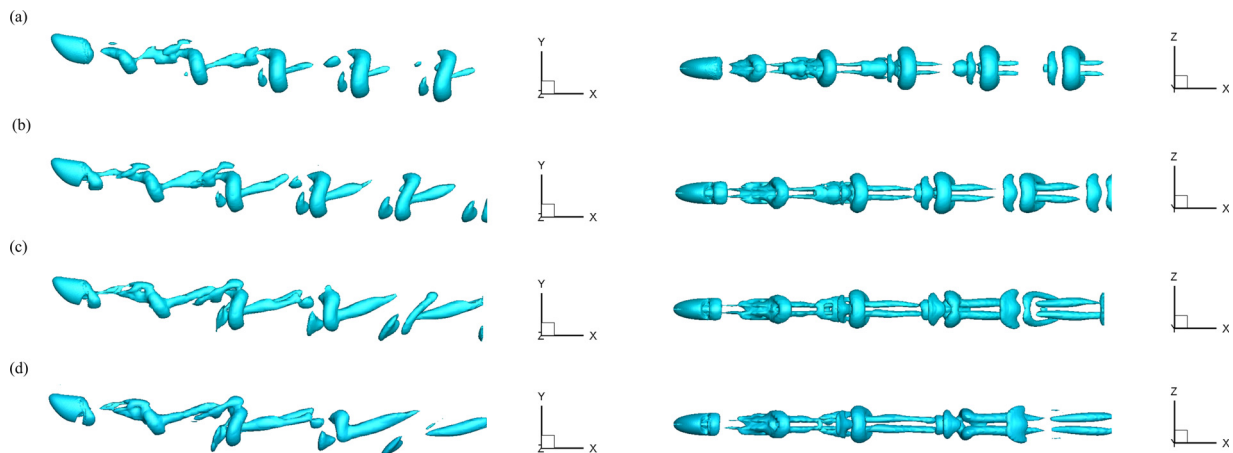


FIG. 21. Iso-surfaces of Q (two orthogonal views, $QD_e^2/U_c^2 = 2.2 \times 10^{-3}$) at $Re = 480$ and $\alpha = -45^\circ$: (a) $K = 0.025$, (b) $K = 0.05$, (c) $K = 0.075$, and (d) $K = 0.1$.

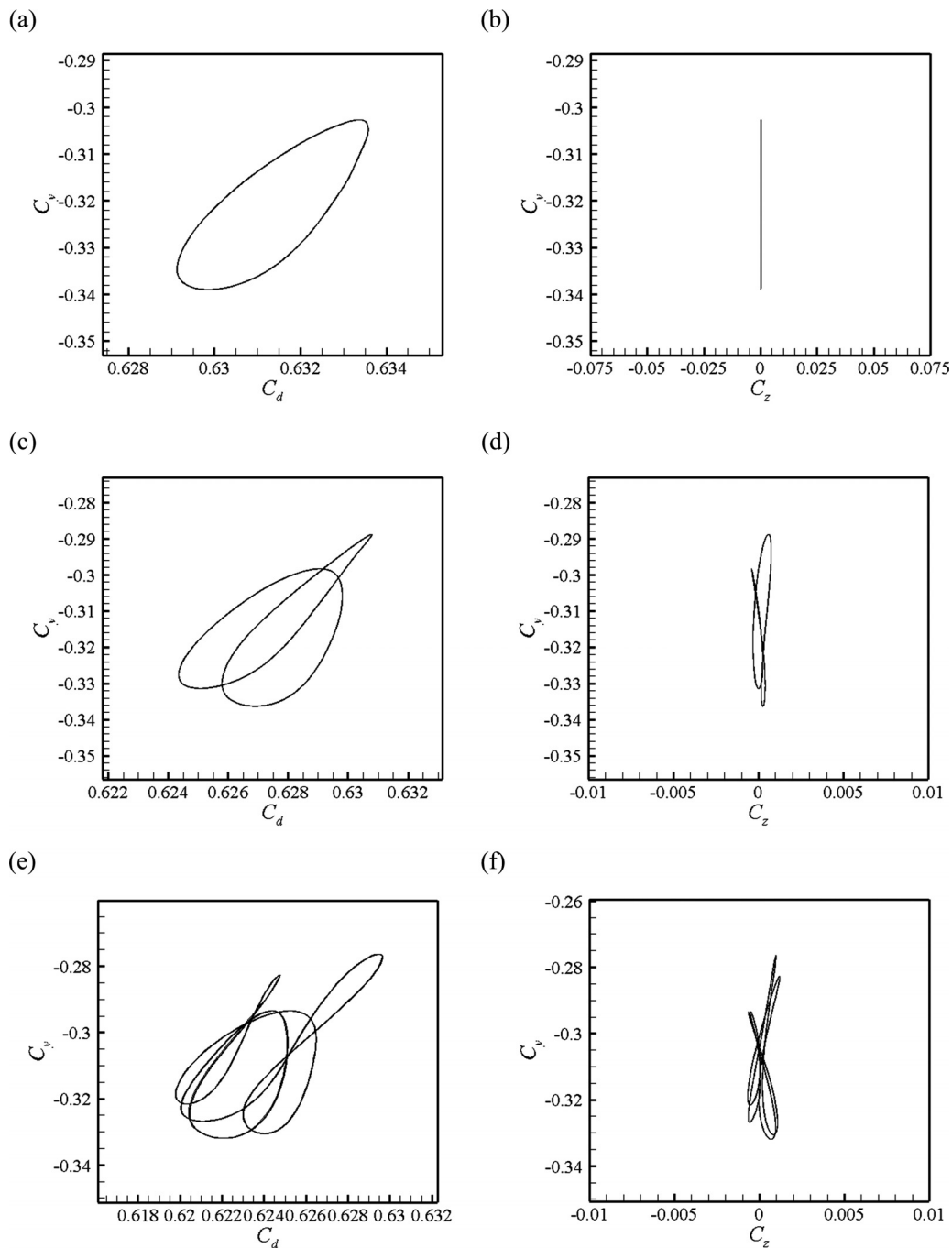


FIG. 22. (a), (c), and (e) $C_d - C_y$ diagram and (b), (d), (f) $C_z - C_y$ diagram at $Re = 480$ and $\alpha = -45^\circ$. (a) and (b) $K = 0.05$, (c) and (d) $K = 0.075$, and (e) and (f) $K = 0.1$.

almost linearly with increasing shear rate K , in contrast to the non-linearly increasing drag for $\alpha = +45^\circ$, as shown in Fig. 24(a). Aside from the obviously different directions of the lift force, the lift coefficient decreases with K for $\alpha = -45^\circ$, in contrast to the increasing magnitude of the lift coefficient for $\alpha = +45^\circ$, as shown in Fig. 24(b). Due to the steady wake for $K = 0.075$ and 0.1 at $\alpha = +45^\circ$, there are only

three data points for the Strouhal number in Fig. 24(c), which show an increase with increasing shear rate K . For $\alpha = -45^\circ$, however, the Strouhal number shows a decreasing trend with increasing shear rate, in contrast to the wake of a sphere. The above results show that the sign of the incidence angle, i.e., whether positive or negative, has a decisive impact on the evolution of the wake of an inclined spheroid in

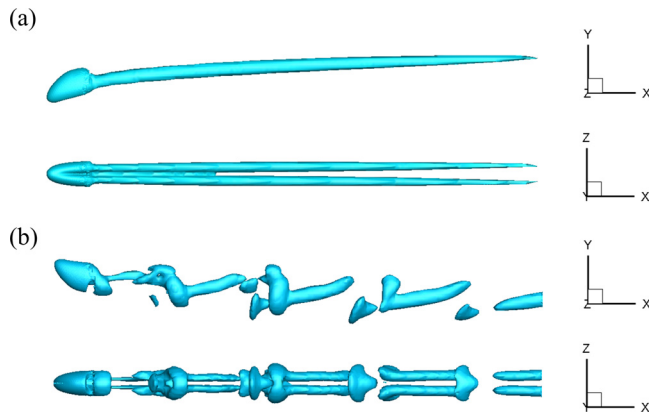


FIG. 23. (a) Steady planar-symmetric flow regime at $Re = 400$ and $K = 0.1$ for $\alpha = +45^\circ$, iso-surface of Q (two orthogonal views), $QD_e^2/U_c^2 = 9.9 \times 10^{-3}$ and (b) unsteady planar-symmetric flow regime at $Re = 400$ and $K = 0.1$ for $\alpha = -45^\circ$, iso-surface of Q (two orthogonal views), $QD_e^2/U_c^2 = 2.2 \times 10^{-3}$.

a uniform shear flow. We now aim to provide a physical explanation on this phenomenon.

As already suggested, two different local Reynolds numbers may be introduced in a uniform shear flow, namely, the Reynolds number at the leading-edge side of the prolate spheroid (L-Re) and the Reynolds number at the trailing-edge side of the spheroid (T-Re). The leading edge of the prolate spheroid at $\alpha = +45^\circ$ is at the low-velocity side of the shear flow, while the trailing edge of the spheroid is at the high-velocity side. With increasing shear rate, the leading-edge velocity of the prolate spheroid is further decreased while the trailing-edge velocity is increased. On the contrary, at $\alpha = -45^\circ$, the leading edge of the prolate spheroid is at the high-velocity side of the shear flow while the trailing edge of the spheroid is located at the low-velocity side. With an increase in the shear rate, the leading-edge velocity of the prolate spheroid is further increased. As mentioned before, the trends of the drag and lift coefficients at $\alpha = 45^\circ$ and $\alpha = -45^\circ$ are opposite with the drag and lift coefficients increasing at $\alpha = +45^\circ$ while decreasing at $\alpha = -45^\circ$ with increasing shear rate K . In some earlier studies,^{33,45,46} the effect of an increasing Reynolds number on the drag and lift coefficients of a 5:2 prolate spheroid in a uniform flow is to

decrease the drag and lift coefficients. It suggests that the drag and lift forces are mainly determined by the Reynolds number at the leading-edge side of the prolate spheroid. The change in the local Reynolds number at the leading-edge side of the prolate spheroid is related to the flow state and wake structures and, thus, would lead to the change in the drag/lift coefficient.

The distribution of the local Reynolds numbers around the prolate spheroid with positive incidence $\alpha = +45^\circ$ is shown in Fig. 25 for different shear rates. Two regions with locally high Reynolds numbers are observed around the leading and trailing-edge sides of the spheroid and apparently related to vortex shedding. In uniform inflow, the time evolution in Fig. 26 shows that the whole vortex loop is shedding due to interactions between the separated shear layers at the leading and trailing edges of the prolate spheroid. However, the variation in the vortex shedding frequency is mainly controlled by T-Re, i.e., the Reynolds number at the vortex-shedding side. At $\alpha = +45^\circ$, the increasing vortex shedding frequency with increasing shear rate is probably due to the increase in the trailing-edge Reynolds number, which in turn leads to higher vorticity entrained into the vortex formation region, similarly as in the wake of a sphere wake. Contrary to the sphere wake, however, the present flow reverts from unsteady to the steady at high shear rates. It might be due to an effect of the distinct decrease in the leading-edge Reynolds number observed in Figs. 25(d) and 25(e). The differences in the velocity distributions along the surface of the prolate spheroid are relatively larger than along a sphere. Moreover, due to the incidence angle, the vortex shedding always occurs near the trailing edge of the spheroid. This indicates that the shear layer vorticity separating from the surface of the spheroid concentrates in the vortex formation region of the trailing edge. At $\alpha = +45^\circ$ with increasing shear rate K , the leading-edge velocity of the prolate spheroid is gradually decreased, which can bring about a decrease in vorticity separating from the leading edge of the prolate spheroid. Meanwhile, due to the increase in the trailing-edge velocity of the prolate spheroid, the vortex shedding frequency is increased and more vorticity needs to be supplied to the vortex formation region. Therefore, the balance between supply and emission of vorticity is broken, which makes the flow return to steady state. For $\alpha = -45^\circ$, the trailing edge of the prolate spheroid locates at the low-velocity side. With an increase in the inflow shear rate, the trailing-edge velocity is decreased causing a reduction in vorticity entrained into the vortex

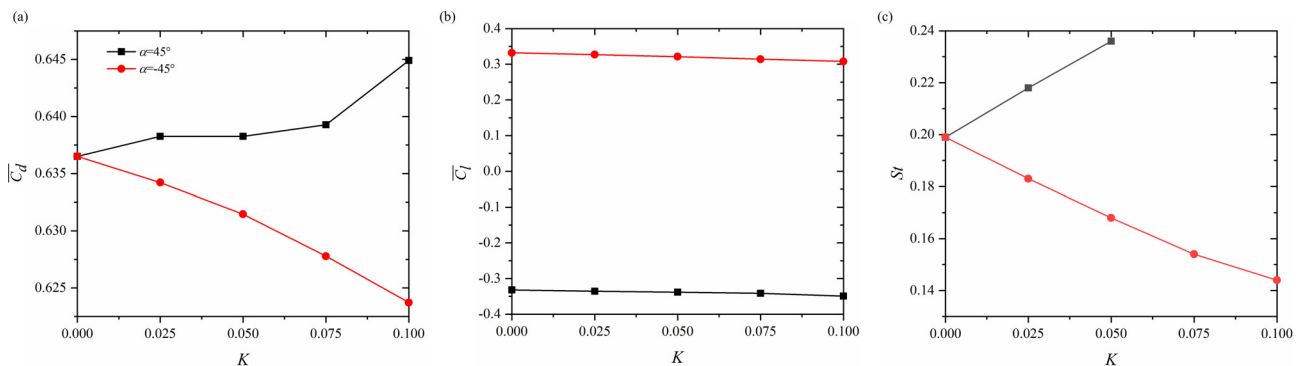


FIG. 24. Variations of the time-averaged drag, lift coefficients, and Strouhal number for different shear rates K and incidence angles α at $Re = 480$ (a) drag coefficient, (b) lift coefficient, and (c) Strouhal number. —■—, $\alpha = 45^\circ$; —●—, $\alpha = -45^\circ$.

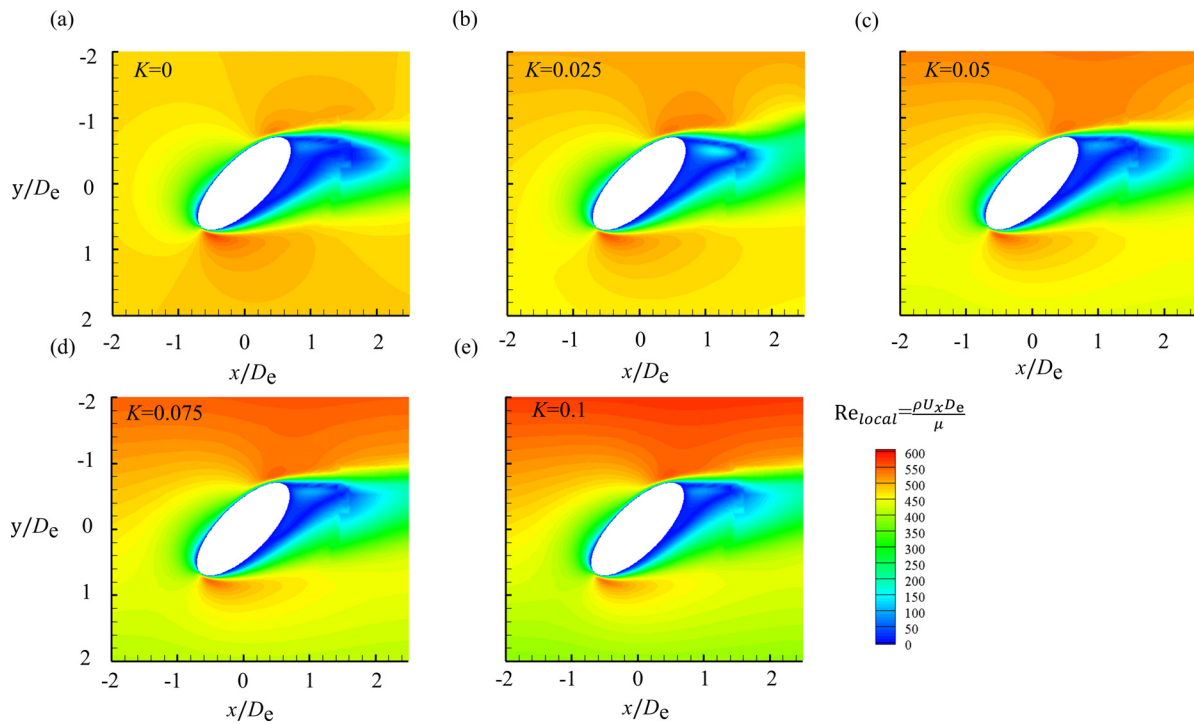


FIG. 25. Contours of the local Reynolds number near the spheroid for $\alpha = +45^\circ$ and $Re = 480$ for different shear rates at the xoy plane: (a) $K = 0$, (b) $K = 0.025$, (c) $K = 0.05$, (d) $K = 0.075$, and (e) $K = 0.1$.

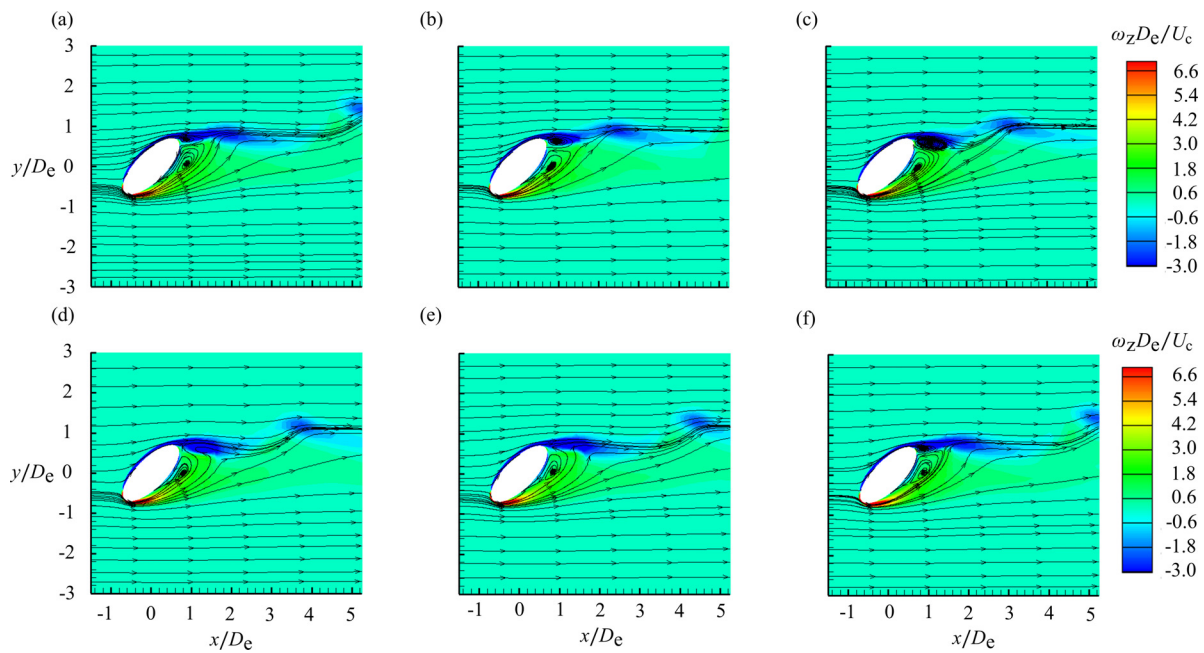


FIG. 26. Time sequence of the vortex shedding process characterized by iso-surfaces of z-vorticity, ω_z , and in-plane streamlines in the xoz plane at $\alpha = +45^\circ$ and $Re = 480$ and $K = 0$: (a) $t = 0$, (b) $t = 1.005 D_e / U_c$, (c) $t = 2.01 D_e / U_c$, (d) $t = 3.015 D_e / U_c$, (e) $t = 4.02 D_e / U_c$, and (f) $t = 5.025 D_e / U_c$.

formation region, which suppresses the formation of vortices and leads to a decrease in the vortex shedding frequency. Moreover, since the leading edge of the prolate spheroid locates at the high-velocity side, sufficient vorticity is supplied to the trailing edge. With further increase in the shear rate K , the more vorticity from the separated shear layer is rolling up from the high-velocity side and supplied to the vortex shedding region, causing the asymmetry of the wake structure.

In summary, in a uniform shear flow, the evolution of the wake of an inclined prolate spheroid depends on the inclination direction of the spheroid, which introduces two different local Reynolds numbers, i.e., L-Re and T-Re. The leading-edge Reynolds number determines the flow state, i.e., steady state or unsteady state. When the leading-edge Reynolds number is sufficiently low, the flow even reverts from unsteady to steady. Moreover, the leading-edge Reynolds number also affects the variation of the drag and lift coefficients. When the leading edge of the prolate spheroid locates at the high-velocity side, the drag and lift coefficients are decreased with the increase in the shear rate K , similarly to the decrease observed with increasing Re in uniform flow ($K=0$). When the leading edge of the prolate spheroid locates at the low-velocity side, the drag and lift coefficients are increased with the increase in the shear rate, analogously with the increase with decreasing Re in uniform flow. The trailing-edge Reynolds number affects the variation of the vortex shedding frequency. When the trailing edge of the prolate spheroid locates at the high-velocity side, the vortex shedding frequency is increased with increasing K . When the trailing edge of the prolate spheroid locates at the low-velocity side, the vortex shedding frequency is decreased with an increase in the shear rate.

IV. CONCLUSIONS

Flow around a 5:2 prolate spheroid with the incidence angle $\alpha = 45^\circ$ in a uniform shear flow is numerically investigated. The Reynolds number ($Re = 480, 600, 700$, and 750) and the non-dimensional shear rate ($K = 0-0.1$) are the two parameters affecting the wake evolution, where Re and K are based on the inflow velocity at the geometric center U_c and the volume-equivalent sphere diameter D_e of the spheroid. Five qualitatively different wake modes are observed, i.e., the steady-state (SS) mode, Zig-zig (Zz) mode, quasi-periodic asymmetric mode (QPA), multi-periodic asymmetric mode (MPA), and multi-periodic shedding of the hairpin vortex with regular rotation of the separation region (MPRRS), where the last mode is observed for the first time. Generally, with increasing shear rate, the vortex shedding is suppressed due to the fixed vortex detachment point on the high-velocity side maintaining the balance between the supply and emission of vorticity within the vortex formation region. At $Re = 480$, in particular, the flows change from unsteady to steady states at high shear rates, which can be attributed to the breaking of the balance between supply and emission of vorticity due to the obvious reduction of the leading-edge Reynolds number. At higher Reynolds numbers, a further increase in the shear rate also promotes wake transition. At $Re = 700$, the flow changes from an unsteady asymmetric state to an unsteady planar symmetric state and then returns to the unsteady asymmetric state with gradually increasing shear rate. The absolute value of the time-averaged drag, lift coefficients, and the Strouhal number increased with increasing shear rate. The time-averaged drag and lift coefficients decreased with increasing Reynolds number. The Strouhal number increased with increasing Reynolds number at different shear rates, except for $K = 0$ when the

Strouhal number is first increased and thereafter decreased. This is attributed to the relatively chaotic flow state at higher Reynolds numbers.

Finally, the effect of negative vs positive incidence angle on the evolution of the wake behind the prolate spheroid was investigated at $Re = 480$. The variations of drag and lift coefficients are determined by the leading-edge Reynolds number, similar to those in a uniform flow. When $\alpha = +45^\circ$, the leading edge of the prolate spheroid locates at the low-velocity side, and the leading-side Reynolds number is, thus, decreased with the increase in the shear rate. This leads to an increase in the drag and lift coefficients as in a uniform flow. When $\alpha = -45^\circ$, the leading edge of the prolate spheroid locates at the high-velocity side, and the leading-side Reynolds number becomes higher with increasing shear rate. Therefore, the drag and lift coefficients decrease as in uniform flow. The trailing-edge Reynolds number affects the variation of the vortex shedding frequency. When $\alpha = +45^\circ$, the trailing edge of the prolate spheroid locates at the high-velocity side, and a higher vortex shedding frequency occurs when shear rates increase, which can be attributed to the higher vorticity entrained into the vortex formation region. When $\alpha = -45^\circ$, however, the trailing edge of the prolate spheroid locates at the low-velocity side, and the vortex shedding frequency is decreased with the increase in the shear rate, caused by the reduced vorticity entrained in the vortex formation region.

ACKNOWLEDGMENTS

The research presented in this paper was partially supported by the Natural Science Foundation of China (Nos. 11947012 and 51806001), the Anhui Provincial Natural Science Foundation (No. 1908085MA08), Fundamental Research Funds for the Central Universities (No. JZ2021HGTB0122), and the Foundation of National Key Laboratory of Science and Technology on Aerodynamic Design and Research (No. 614220121030223). The numerical calculations in this paper have been done on the supercomputing system in the Supercomputing Center of University of Science and Technology of China.

AUTHOR DECLARATIONS

Conflict of Interest

The authors have no conflicts to disclose.

DATA AVAILABILITY

The data that support the findings of this study are available from the corresponding author upon reasonable request.

REFERENCES

- ¹M. Chrust, S. Goujon-Durand, and J. E. Wesfreid, "Loss of a fixed plane of symmetry in the wake of a sphere," *J. Fluid Struct.* **41**, 51–56 (2013).
- ²D. Fabre, F. Auguste, and J. Magnaudet, "Bifurcations and symmetry breaking in the wake of axisymmetric bodies," *Phys. Fluids* **20**, 051702 (2008).
- ³B. Ghidersa and J. A. N. Dušek, "Breaking of axisymmetry and onset of unsteadiness in the wake of a sphere," *J. Fluid Mech.* **423**, 33–69 (2000).
- ⁴T. A. Johnson and V. C. Patel, "Flow past a sphere up to a Reynolds number of 300," *J. Fluid Mech.* **378**, 19–70 (1999).
- ⁵R. H. Magarvey and R. L. Bishop, "Transition ranges for three-dimensional wakes," *Can. J. Phys.* **39**, 1418–1422 (1961).

- ⁶R. Mittal, "Planar symmetry in the unsteady wake of a sphere," *AIAA J.* **37**, 388–390 (1999).
- ⁷I. Nakamura, "Steady wake behind a sphere," *Phys. Fluids* **19**, 5 (1976).
- ⁸R. Natarajan and A. Acrivos, "The instability of the steady flow past spheres and disks," *J. Fluid Mech.* **254**, 323–344 (1993).
- ⁹I. Kim and A. J. Pearlstein, "Stability of the flow past a sphere," *J. Fluid Mech.* **211**, 73–93 (1990).
- ¹⁰B. Pier, "Local and global instabilities in the wake of a sphere," *J. Fluid Mech.* **603**, 39–61 (2008).
- ¹¹H. Sakamoto and H. Haniu, "A study on vortex shedding from spheres in a uniform flow," *J. Fluids Eng.* **112**, 386–392 (1990).
- ¹²S. Taneda, "Experimental investigation of the wake behind a sphere at low Reynolds numbers," *J. Phys. Soc. Jpn.* **11**, 1104 (1956).
- ¹³A. G. Tomboulides and S. A. Orszag, "Numerical investigation of transitional and weak turbulent flow past a sphere," *J. Fluid Mech.* **416**, 45–73 (2000).
- ¹⁴X. Xiang, K. Chen, T. Madison, P. Sellappan, and G. Spedding, "Experiments and simulations of low Re sphere wakes with and without stratification," *Int. Symp. Stratified Flows* **1**, 1–7 (2016).
- ¹⁵D. S. Dandy and H. A. Dwyer, "A sphere in shear flow at finite Reynolds number: Effect of shear on particle lift, drag, and heat transfer," *J. Fluid Mech.* **216**, 381–410 (1990).
- ¹⁶D. Kim, H. Choi, and H. Choi, "Characteristics of laminar flow past a sphere in uniform shear," *Phys. Fluids* **17**, 103602 (2005).
- ¹⁷S. Lee and J. M. Wilczak, "The effects of shear flow on the unsteady wakes behind a sphere at moderate Reynolds numbers," *Fluid Dyn. Res.* **27**, 1–22 (2000).
- ¹⁸J. B. McLaughlin, "Inertial migration of a small sphere in linear shear flows," *J. Fluid Mech.* **224**, 261–274 (1991).
- ¹⁹P. G. Saffman, "The lift on a small sphere in a slow shear flow," *J. Fluid Mech.* **22**, 385–400 (1965).
- ²⁰H. Sakamoto and H. Haniu, "The formation mechanism and shedding frequency of vortices from a sphere in uniform shear flow," *J. Fluid Mech.* **287**, 151–171 (1995).
- ²¹L. Zeng, S. Balachandar, and P. Fischer, "Wall-induced forces on a rigid sphere at finite Reynolds number," *J. Fluid Mech.* **536**, 1–25 (2005).
- ²²L. Zeng, F. Najjar, S. Balachandar, and P. Fischer, "Forces on a finite-sized particle located close to a wall in a linear shear flow," *Phys. Fluids* **21**, 033302 (2009).
- ²³Y. Shiliang, H. Site, and Z. Wentao, "Mixing and dispersion behaviours of ellipsoid particles in a bubbling fluidized bed," *Powder Technol.* **396**, Part A, 210–223 (2022).
- ²⁴J. Heo, J. Kim, and Y. Kwon, "Technology development of unmanned underwater vehicles (UUVs)," *J. Comput. Commun.* **05**, 28–35 (2017).
- ²⁵G. R. Hall, "Interaction of the wake from bluff bodies with an initially laminar boundary layer," *AIAA J.* **5**, 1386–1392 (1967).
- ²⁶A. A. Zamyshlyayev and G. R. Shrager, "Fluid flows past spheroids at moderate Reynolds numbers," *Fluid Dyn.* **39**, 376–383 (2004).
- ²⁷G. K. El Khoury, H. I. Andersson, and B. Pettersen, "Wakes behind a prolate spheroid in crossflow," *J. Fluid Mech.* **701**, 98–136 (2012).
- ²⁸F. Jiang, J. P. Gallardo, and H. I. Andersson, "The laminar wake behind a 6:1 prolate spheroid at 45° incidence angle," *Phys. Fluids* **26**, 113602 (2014).
- ²⁹F. Jiang, H. I. Andersson, J. P. Gallardo, and V. L. Okulov, "On the peculiar structure of a helical wake vortex behind an inclined prolate spheroid," *J. Fluid Mech.* **801**, 1–12 (2016).
- ³⁰F. Jiang, J. P. Gallardo, H. I. Andersson, and Z. Zhang, "The transitional wake behind an inclined prolate spheroid," *Phys. Fluids* **27**, 093602 (2015).
- ³¹H. I. Andersson, F. Jiang, and V. L. Okulov, "Instabilities in the wake of an inclined prolate spheroid," in *Computational Modelling of Bifurcations and Instabilities in Fluid Dynamics*, Part of the Computational Methods in Applied Sciences Book Series (Springer, 2018).
- ³²H. Strandén, F. Jiang, B. Pettersen, and H. I. Andersson, "Near-wake of an inclined 6:1 spheroid at Reynolds number 4000," *AIAA J.* **57**, 1364–1372 (2019).
- ³³Z. Wang *et al.*, "Numerical investigation on the flow around an inclined prolate spheroid," *Phys. Fluids* **33**, 074106 (2021).
- ³⁴A. Hölzer and M. Sommerfeld, "Lattice Boltzmann simulations to determine drag, lift and torque acting on non-spherical particles," *Comput. Fluids* **38**, 572–589 (2009).
- ³⁵P. Fillingham, R. S. Vaddi, A. Bruning, G. Israel, and I. V. Novosselov, "Drag, lift, and torque on a prolate spheroid resting on a smooth surface in a linear shear flow," *Powder Technol.* **377**, 958–965 (2021).
- ³⁶J. Jeong and F. Hussain, "On the identification of a vortex," *J. Fluid Mech.* **285**, 69–94 (1995).
- ³⁷J. Yang, M. Liu, C. Wang, X. Zhu, and A. Zhang, "Numerical study on uniform-shear flow over a circular disk at low Reynolds numbers," *Phys. Fluids* **30**, 083605 (2018).
- ³⁸F. Auguste, D. Fabre, and J. Magnaudet, "Bifurcations in the wake of a thick circular disk," *Theor. Comput. Fluid Dyn.* **24**, 305–313 (2010).
- ³⁹S. Gao, L. Tao, X. Tian, and J. Yang, "Flow around an inclined circular disk," *J. Fluid Mech.* **851**, 687–714 (2018).
- ⁴⁰X. Tian, Z. Hu, H. Lu, and J. Yang, "Direct numerical simulations on the flow past an inclined circular disk," *J. Fluid Struct.* **72**, 152–168 (2017).
- ⁴¹Q. Meng, H. An, L. Cheng, and M. Kimiaei, "Wake transitions behind a cube at low and moderate Reynolds numbers," *J. Fluid Mech.* **919**, A44 (2021).
- ⁴²S. R. Kumar, A. Sharma, and A. Agrawal, "Simulation of flow around a row of square cylinders," *J. Fluid Mech.* **606**, 369–397 (2008).
- ⁴³A. Sanyal and A. Dhiman, "Wake interactions in a fluid flow past a pair of side-by-side square cylinders in presence of mixed convection," *Phys. Fluids* **29**, 103602 (2017).
- ⁴⁴C. M. Sewatkar, R. Patel, A. Sharma, and A. Agrawal, "Flow around six in-line square cylinders," *J. Fluid Mech.* **710**, 195–233 (2012).
- ⁴⁵S. K. P. Sanjeevi, J. A. M. Kuipers, and J. T. Padding, "Drag, lift and torque correlations for non-spherical particles from Stokes limit to high Reynolds numbers," *Int. J. Multiphase Flow* **106**, 325–337 (2018).
- ⁴⁶M. Zastawny, G. Mallouppas, F. Zhao, and B. van Wachem, "Derivation of drag and lift force and torque coefficients for non-spherical particles in flows," *Int. J. Multiphase Flow* **39**, 227–239 (2012).